REPORT 1253

A CORRELATION BY MEANS OF TRANSONIC SIMILARITY RULES OF EXPERIMENTALLY DETERMINED CHARACTERISTICS OF A SERIES OF SYMMETRICAL AND CAMBERED WINGS OF RECTANGULAR PLAN FORM [1]

By JOHN B. MCDEVITT

SUMMARY

Transonic similarity rules are applied to the correlation of experimental data for a series of related rectangular wings of varying aspect ratio, thickness, and camber. The data correlation is presented in two parts: The first part presents the correlation for a series of 22 wings having symmetrical NACA 63A-series sections; the second part is concerned with a study of one type of camber by correlation of the data for a series of 18 cambered wings having NACA 63A2XX and 63A4XX sections.

It was found that the experimental data could be, for the most part, successfully correlated throughout the subsonic, transonic, and moderate supersonic regimes and that, by proper choice of parameters, the force and moment data could be presented in a concise manner effectively displaying the transonic characteristics of wings of both large and small aspect ratios. In many instances it was found possible to predict from the correlation studies an expected range of validity for the linearized or slender-body theories. It appears that at the sonic speed, slender-body theory is adequate for rectangular wings of symmetrical profile if the product of the aspect ratio and the 1/3 power of the thickness ratio is less than unity.

INTRODUCTION

Recent systematic experimental investigations of the effects of wing aspect ratio, thickness, and camber for wings of rectangular plan form at transonic speeds (refs. 1 and 2) have provided data ideally suited for correlation by means of the transonic similarity parameters (refs. 3 to 12). A data-correlation study for wings of symmetrical profiles was made in reference 8 and a similar study for wings of cambered profiles in reference 9. The present report presents the more important results of these two correlation studies.

SYMBOLS

A	aspect ratio, $\frac{b}{c}$
b	wing span
c	wing chord
C_D	total drag coefficient, $\frac{\text{total drag}}{gS}$
$C_{D_{min}}$	minimum drag coefficient
C_{D_f}	friction-drag coefficient, assumed equal to minimum drag coefficient at 0.7 Mach number
$(C_{D_p})_{min}$	minimum pressure-drag coefficient, $C_{D_{min}}-C_{D_f}$
$C_{D_{int}}$	intercept drag coefficient for cambered wings (See fig. 21.)
$(C_{D_p})_{int}$	intercept pressure-drag coefficient for cambered wings (See fig. 21.)
ΔC_D	drag coefficient due to lift, $C_D-C_{D_{min}}$ or $C_D-C_{D_{int}}$
C_L	lift coefficient, $\frac{\text{lift}}{gS}$
$C_{L_{opt}}$	lift coefficient for maximum lift-drag ratio
C_m	pitching-moment coefficient, referred to $0.25c$, $\frac{\text{pitching moment}}{gSc}$
$C.P.$	center of pressure
C_p	pressure coefficient
$\mathcal{D}$	drag function
h	camber, maximum displacement of profile mean line from chord line (See fig. 18.)
$\mathcal{L}$	lift function
$\left(\frac{L}{D}\right)_{max}$	maximum lift-drag ratio
M	free-stream Mach number
M_{cr}	critical Mach number
$\mathcal{M}$	pitching-moment function
$\mathcal{P}$	pressure function
g	dynamic pressure
S	wing area
$\frac{t}{c}$	thickness-to-chord ratio
x,y,z	Cartesian coordinates where x extends in the direction of the free-stream velocity
u,v,w	perturbation velocities normalized by division by the free-stream velocity
α	angle of attack
α_o	angle of attack for zero lift
γ	ratio of specific heats (for air $\gamma=1.4$)
τ	ordinate-amplitude parameter
φ	perturbation-velocity potential normalized by division by the free-stream velocity
$\frac{dC_L}{d\alpha}$	slope of lift curve, measured at zero lift
$\frac{dC_m}{dC_L}$	slope of pitching-moment curve

[1] Supersedes NACA RM A51L17b, 1952, and NACA RM A53G31, 1953, by John B. McDevitt.

TRANSONIC SIMILARITY RULES

RELATIONSHIPS FOR POTENTIAL FLOW

The similarity law for the two-dimensional potential flow about thin related wings at near sonic speeds was first published by von Kármán, reference 3. (See also refs. 4 and 5.) The extension of this law to include wings of finite span was made by Berndt (ref. 6) and by Spreiter (ref. 7). According to reference 7 the pressure coefficient can be expressed in the symbolic form [2]

$$C_p=\frac{\tau^{2/3}}{(\gamma+1)^{1/3}}\mathcal{P}\left\{\frac{M^2-1}{[(\gamma+1)\tau]^{2/3}},(M^2-1)A^2;\frac{x}{c},\frac{y}{b}\right\} \tag{1}$$

where τ is an "ordinate-amplitude" parameter used to denote changes in profile thickness, angle of attack, or camber. This form of the similarity rule is inconvenient for use in the correlation of experimental data since the two parameters $\frac{M^2-1}{[(\gamma+1)\tau]^{2/3}}$ and $(M^2-1)A^2$ vanish at $M=1$. However, as was recognized by Berndt, one can take the ratio of the two parameters to obtain an alternative parameter which does not vanish at $M=1$. The fundamental importance of the alternative parameter $A(t/c)^{1/3}$ was originally demonstrated by the data-correlation study of reference 8. In recent years several papers concerned with the application of transonic similarity rules have been published (e. g., refs. 10 to 12).

The potential equation of small-disturbance theory which is valid for wings of moderate or small aspect ratio and for unswept wings of large aspect ratio is the following

$$(1-M^2)\varphi_{xx}+\varphi_{yy}+\varphi_{zz}=(\gamma+1)M^2\varphi_x\varphi_{xx} \tag{2}$$

The similarity rule based on equation (2) is the following (ref. 10):

$$\frac{[(\gamma+1)M^2]^{1/3}}{\tau^{2/3}}C_p=\mathcal{P}\left\{\frac{M^2-1}{[(\gamma+1)M^2\tau]^{2/3}},A[(\gamma+1)M^2\tau]^{1/3};\frac{x}{c},\frac{y}{b}\right\} \tag{3}$$

$$\tau\sim\frac{t}{c},\frac{h}{c},\text{ or }\alpha$$

When considering a particular class of similar wings it is possible to write equation (3) in the more convenient form

$$\frac{[(\gamma+1)M^2]^{1/3}}{\tau^{2/3}}C_p=\mathcal{P}\left\{\frac{M^2-1}{[(\gamma+1)M^2t/c]^{2/3}},A[(\gamma+1)M^2t/c]^{1/3},\frac{\alpha}{t/c},\frac{h}{t}\right\} \tag{4}$$

where τ in the left-hand expression can be replaced by t/c h/c, or α, depending on the particular problem at hand. Furthermore, it should be recognized that the left-hand side of equation (4) can be modified by multiplication or division by any of the parameters within the brackets, or by any combination of the parameters.

[2] In the early literature concerning transonic flow theory various forms of the similarity rules were given, all of which are equivalent at a Mach number of 1 but differ slightly at nonsonic Mach numbers, according to the assumptions made in obtaining the fundamental equations.

INVARIANT RELATIONSHIPS FOR THE SHOCK POLAR

Since shock waves invariably appear in the mixed subsonic-supersonic flow that surrounds an airfoil at transonic speeds, it is necessary that the essential properties of shock waves depend on the same similarity parameters as does the continuous potential flow if a successful application of the similarity rules is to be made in the correlation of experimental data at transonic speeds.

When a uniform flow of velocity U_1 is assumed parallel to the x axis and if the velocity components after the shock are designated by U_2 and W_2, then the classical shock polar, according to Busemann, (e. g., ref. 13, p. 53), is

$$W_2^2=(U_1-U_2)^2\frac{U_1U_2-a^{*2}}{\frac{2}{\gamma+1}U_1^2-U_1U_2+a^{*2}} \tag{5}$$

where a^* is the critical speed of sound. By defining the velocity perturbations to be the ratios

$$\bar{u}=\frac{U_2-U_1}{U_1},\ \bar{w}=\frac{W_2}{U_1} \tag{6}$$

the shock polar can be written as

$$\bar{w}^2=\frac{(M_1^2-1)\bar{u}^2+\frac{\gamma+1}{2}M_1^2\bar{u}^3}{1-\frac{\gamma+1}{2}M_1^2\bar{u}} \tag{7}$$

where M_1 is the Mach number ahead of the shock. For Mach numbers slightly greater than 1 an approximation for equation (7) can be obtained in the following manner. At transonic speeds velocity perturbations normal to the free-stream direction can be considered to be of smaller order than velocity perturbations in the free-stream direction; that is,

$$\bar{w}<\bar{u}$$

Then, if equation (7) is rewritten in the form

$$\bar{w}^2\left(1-\frac{\gamma+1}{2}M_1^2\bar{u}\right)=(M_1^2-1)\bar{u}^2+\frac{\gamma+1}{2}M_1^2\bar{u}^3$$

and if terms up to the order $\bar{u}^3$ are retained (with terms of order $\bar{u}\bar{w}^2$ neglected), there results

$$(1-M_1^2)\bar{u}^2+\bar{w}^2=\frac{\gamma+1}{2}M_1^2\bar{u}^3 \tag{8}$$

This relationship is exact for normal shocks and for vanishingly weak shocks (Mach waves) and can be considered to be the transonic approximation for the shock polar.

Equation (8) can be written in the invariant form

$$\tilde{\bar{w}}^2=\tilde{\bar{u}}^2+\tilde{\bar{u}}^3 \tag{9}$$

by defining new variables to be

$$\tilde{\bar{u}}=\frac{(\gamma+1)M_1^2\bar{u}}{2(M_1^2-1)},\ \tilde{\bar{w}}=\frac{(\gamma+1)M_1^2\bar{w}}{2(M_1^2-1)^{3/2}}$$

If the usual assumptions of small-disturbance theory ($C_p \sim \bar{u}$ and $\bar{w} \sim \tau$) are made, invariance of the parameter $\frac{M_1^2-1}{[(\gamma+1)M_1^2\tau]^{2/3}}$ leads to invariance of the expression $\frac{[(\gamma+1)M_1^2]^{1/3}}{\tau^{2/3}}C_p$. These parameters are of the same form as those appearing in equation (4).[3]

SIMPLIFIED FORM OF THE TRANSONIC SIMILARITY RULE

The simplified similarity rule given by equation (1) can be written in the form

$$\frac{C_p}{\tau^{2/3}} = \mathcal{P}\left[\frac{M^2-1}{(t/c)^{2/3}}, A\left(\frac{t}{c}\right)^{1/3}, \frac{\alpha}{t/c}, \frac{h}{t}\right] \qquad (10)$$

where the expression $(\gamma+1)$ has been omitted since the gas is assumed to be a constant medium. This expression is equivalent to equation (4) at $M=1$ and can be used equally well when the flow field is entirely subsonic or well-established supersonically since either form can be shown to coincide with the similarity rules of linearized theory. The simplified form has certain advantages, not only because of the relative simplicity of the parameters, but because the particular parameter $A(t/c)^{1/3}$ contains only geometric variables.

For practical reasons, the simplified form of the similarity rule given by equation (10) will be used in the following data correlation since it was found that any improvement of the data correlation resulting from use of the more exact relationship of equation (4) appeared to be within the accuracy of the experimental data. (However, it could be expected that equation (4) would give, in general, superior results when two-dimensional-flow data are compared with nonlinear theory at transonic speeds.)

The variations between Mach number, aspect ratio, and thickness ratio implied by the constancy of the two parameters $\frac{M^2-1}{(t/c)^{2/3}}$ and $A(t/c)^{1/3}$ are shown in figure 1. (See also tables I to III.)

TEST PROCEDURE AND DESCRIPTION OF MODELS

The experimental data for the symmetrical wings (ref. 1) and for the cambered wings, (ref. 2) were obtained by identical testing procedures. The semispan wing models were mounted in the high-velocity field of a bump in the Ames 16-foot high-speed wind tunnel. Although the streamlines of the flow in the testing area were slightly curved, the effects of the nonuniformity of the flow field are believed to be small. However, some rounding off of any sharp breaks in the force and moment variation with Mach number can be expected.

The wings tested were rectangular in plan form and utilized NACA 63A-series profiles. The cambered wings had NACA 63A2XX and 63A4XX sections with an $a=0.8$ (modified) mean line. This modification to the mean line maintained straight portions of the profiles over the last 15 percent of the chord (see ref. 14). The aspect ratio varied from ½ to 6 and the thickness-to-chord ratio varied from 2 to 10 percent. The data were obtained for a Mach number range from 0.40 to 1.10, which corresponded to a Reynolds number range from 1.25 to 2.05 million. A more complete description of the testing procedure is given in the basic data reports, references 1 and 2.

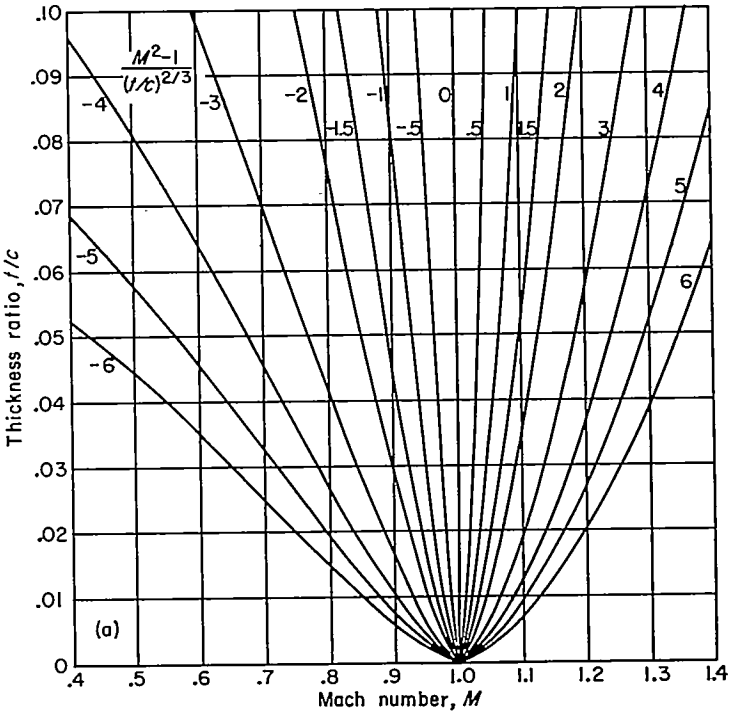

(a) Thickness ratio versus Mach number for constant $\frac{M^2-1}{(t/c)^{2/3}}$.

FIGURE 1.—The transonic similarity parameters.

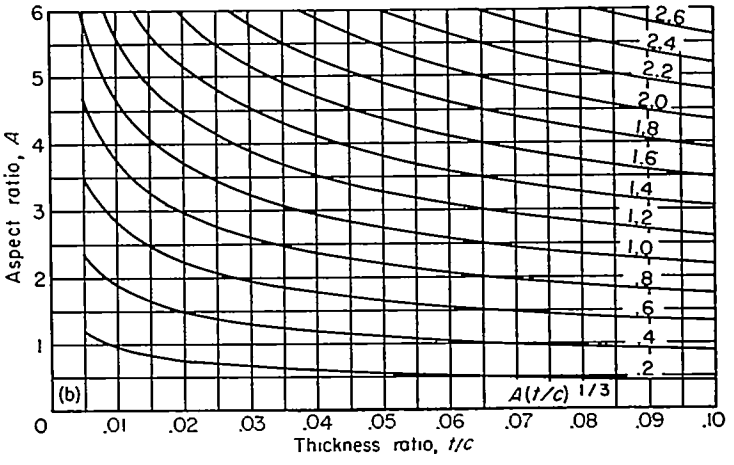

(b) Aspect ratio versus thickness ratio for constant $A(t/c)^{1/3}$.

FIGURE 1.—Concluded.

[3] This discussion can be generalized to include the case when the velocity ahead of the shock is not free stream by use of the following approximate relationship

$$1-M_1^2 \approx 1-M^2-(\gamma+1)M^2\varphi_x$$

If it is assumed that $Cp \sim \bar{u}+\varphi_x$, $\tau \sim \bar{w}+\varphi_z$, and if only terms to the order $\bar{u}^2$ are retained.

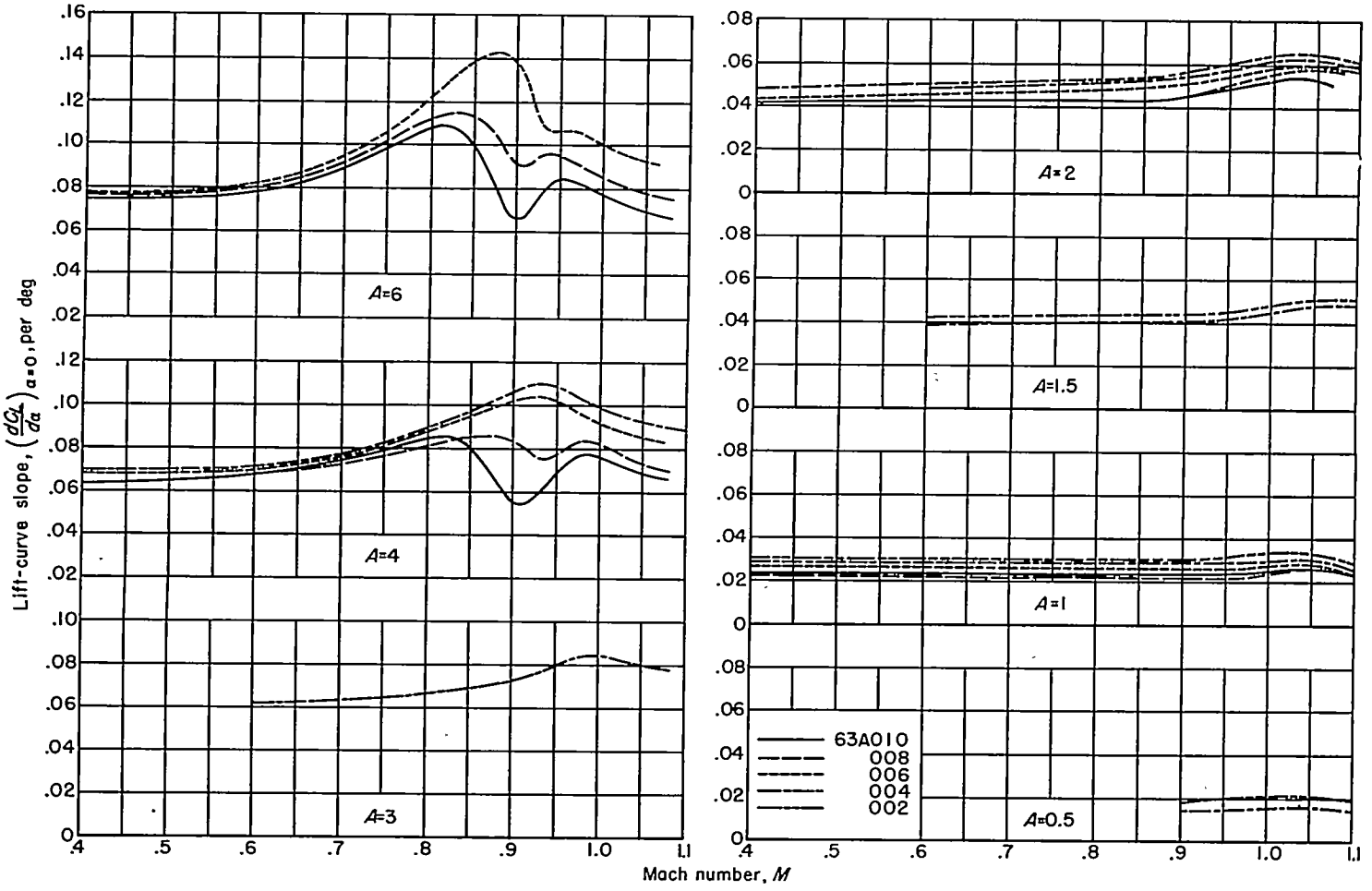

FIGURE 2.—The variation of lift-curve slope with Mach number for the symmetrical wings.

DATA CORRELATION

I. SYMMETRICAL PROFILES

LIFT

The variation of lift coefficient with angle of attack was essentially linear at moderate angles of attack throughout the Mach number range for aspect ratios greater than about 1.5. Although the wings with the lower aspect ratios showed an increasingly nonlinear variation of lift with angle of attack and approached the theoretical $\sin^2 \alpha$ variation for vanishing aspect ratio, it is convenient to restrict the lift analysis to a consideration of the lift-curve slope evaluated at zero-lift coefficient, which provides a close approximation for lift characteristics at the moderate angles of attack for which the similarity rules can be expected to hold.

The variation of lift-curve slope with Mach number is shown in figure 2. Above the critical Mach number an abrupt decrease in lift-curve slope occurred for some of the wings of larger aspect ratio and large thickness ratio. This decrease is believed to be the result of the formation of shock waves which cause flow separation at the airfoil surfaces. As the Mach number approached 1 the shock waves moved toward the wing trailing edges and the flow reattached, resulting in large variations of lift-curve slope with Mach number at high subsonic speeds. This irregular variation in the lift-curve slope is a phenomenon apparently dependent on a combination of thickness and aspect ratio since the smaller thickness ratios and smaller aspect ratios showed no such irregularities in the lift-curve variation with Mach number. (It will be shown in the following data correlation that this erratic variation occurred only for those wings having values of $A(t/c)^{1/3}$ greater than about 1.6.)

In the lift-correlation study the following generalized expression for lift-curve slope is used:

$$\left(\frac{t}{c}\right)^{1/3}\left(\frac{dC_L}{d\alpha}\right)_{\alpha=0}=\mathcal{L}\left[\frac{M^2-1}{(t/c)^{2/3}}, A\left(\frac{t}{c}\right)^{1/3}\right] \qquad (11)$$

$$C_L \sim \alpha$$

The variation of the generalized lift-curve-slope parameter $(t/c)^{1/3}(dC_L/d\alpha)_{\alpha=0}$ with $A(t/c)^{1/3}$ for several constant values of the speed parameter $\frac{M^2-1}{(t/c)^{2/3}}$ is shown in figure 3. Comparison is made for subsonic speeds with the theoretical lift-curve slopes calculated by applying the three-dimensional Prandtl-Glauert transformation to the Weissinger lifting-line theory of reference 15. At $M=1$ comparison is made with the slender-wing theory of R. T. Jones, reference 16. Agreement between theory and experiment for aspect ratios greater than about 3 is satisfactory only in the subcritical Mach number range. At supercritical Mach numbers and values of $A(t/c)^{1/3}$ greater than about 1.6, the poor correlation suggests separated flow for which the concepts of small-perturbation theory would be violated. The value $A(t/c)^{1/3}=1.6$

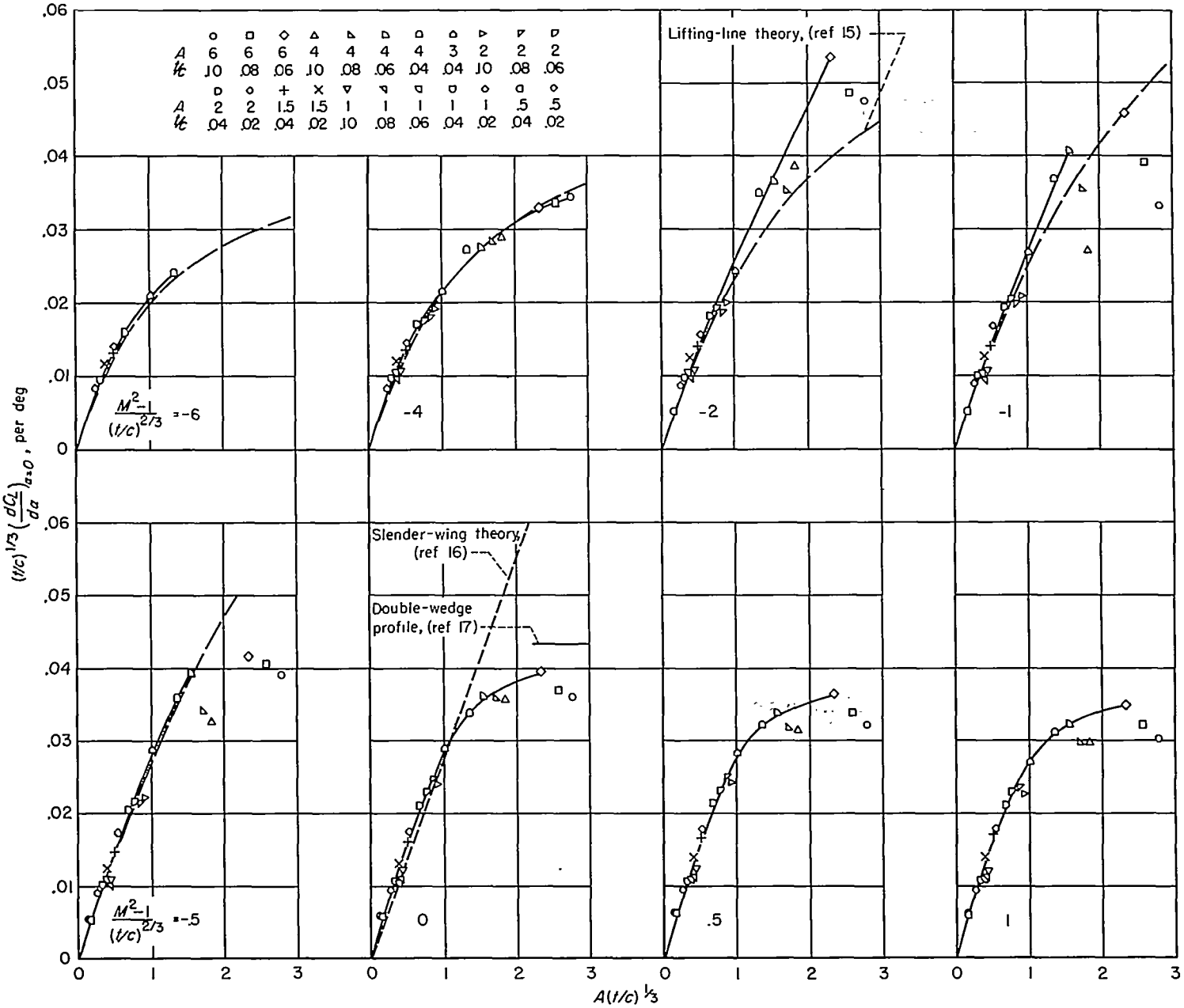

FIGURE 3.—The correlation of lift-curve slope for the symmetrical wings.

appears to be the approximate limit for airfoils which do not exhibit noticeable irregularities in lift-curve-slope variation with Mach number.

At the sonic Mach number $\left(\text{i.e., } \frac{M^2-1}{(t/c)^{2/3}}=0\right)$, the experimental data agree well with slender-wing theory for values of $A(t/c)^{1/3}$ less than about 1. Hence, within the indicated limits, the lift may be approximated by the following equation:

$$C_L=\frac{\pi}{2}A\alpha, \qquad \left.\begin{array}{r} M=1 \\ A\left(\frac{t}{c}\right)^{1/3}<1 \end{array}\right\} \tag{12}$$

For increasingly greater values of $A(t/c)^{1/3}$ a rapid and apparently asymptotic approach of $(t/c)^{1/3}\ (dC_L/d\alpha)_{\alpha=0}$ to a constant value is indicated which implies an inverse variation of lift-curve slope with the 1/3 power of the thickness ratio for sonic, two-dimensional flow. The theoretical result of Guderley and Yoshihara (ref. 17) for a double-wedge profile in sonic, two-dimensional flow is included in figure 3. These results illustrate how the transonic similarity rules can be used to display effectively the transonic characteristics of rectangular wings, showing, in particular, the linear dependence on aspect ratio for small values of $A(t/c)^{1/3}$ and the asymptotic approach toward independence of aspect ratio for large values of $A(t/c)^{1/3}$.

The results of the data correlation are cross-plotted in figure 4 for those values of $A(t/c)^{1/3}$ and $\frac{M^2-1}{(t/c)^{2/3}}$ where a reasonably good correlation was indicated. It is interesting to note that the wings of large $A(t/c)^{1/3}$ exhibit the negative variation of force coefficient with Mach number which is characteristic of two-dimensional flows at sonic speed. This variation is a consequence of the relative variations of local

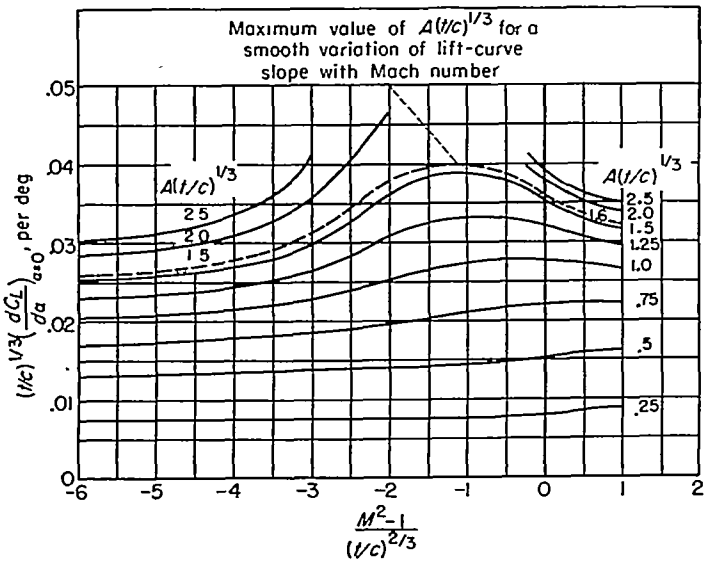

FIGURE 4.—Summary curves of the generalized lift-curve slope for the symmetrical wings.

and free-stream dynamic pressures, the local Mach numbers being effectively frozen at near-sonic values as the free-stream Mach number increases through the transonic speed range. (See refs. 18 to 20.)

DRAG

Whenever possible, it is convenient to separate the drag coefficient into components of friction drag, minimum pressure drag, and drag due to lift,

$$C_D = C_{D_f} + (C_{D_p})_{min} + \Delta C_D \tag{13}$$

The similarity concepts can be applied separately to minimum pressure drag and to drag due to lift but friction drag cannot be brought into the correlation scheme. The friction drag coefficient is believed to change little with Mach number in the transonic range and can be approximated by the minimum drag coefficient at some subcritical Mach number, say at 0.7.

Minimum pressure drag.—The basic data curves for the variation of minimum drag coefficient with Mach number are presented in figure 5. The aspect-ratio-6 wings exhibited the negative variation of force coefficient with Mach number which is characteristic of two-dimensional flow at near sonic speeds. The experimental values of $(dC_D/dM)_{M=1}$ for the wings of aspect ratio 6 agree qualitatively with values implied by the following relationship (an exact theoretical result applicable to symmetrical profiles of any shape, ref. 19):

$$\left(\frac{dC_D}{dM}\right)_{M=1} = -\frac{2}{\gamma+1}(C_D)_{M=1} \tag{14}$$

This agreement occurred in spite of the fact that the test conditions were not ideal and did not agree with the concept of an infinite and uniform flow field assumed in the theoretical reasoning.

The correlation of minimum pressure drag shown in figure 6 was made by application of the following similarity rule

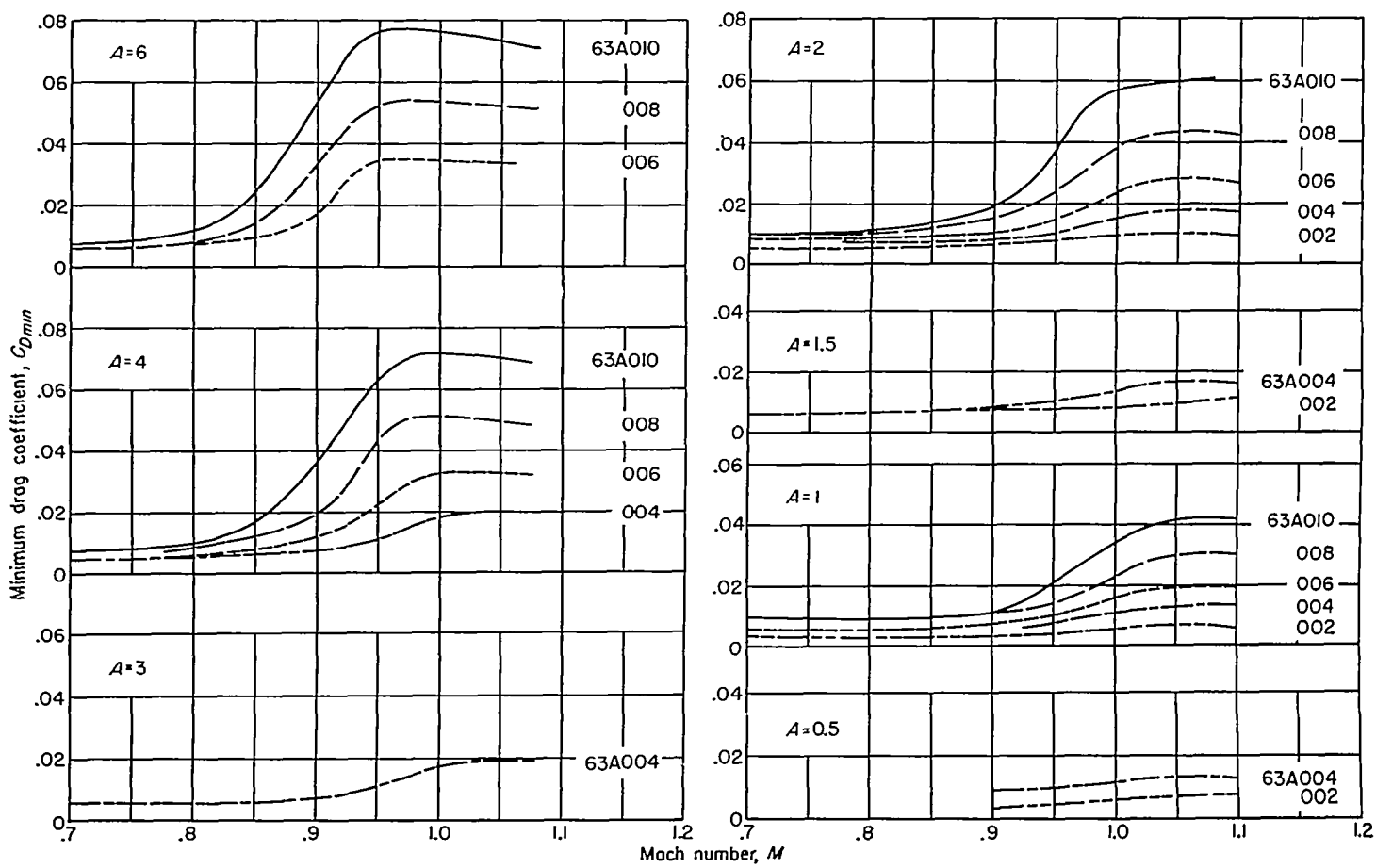

FIGURE 5.—The variation of minimum drag coefficient with Mach number for the symmetrical wings.

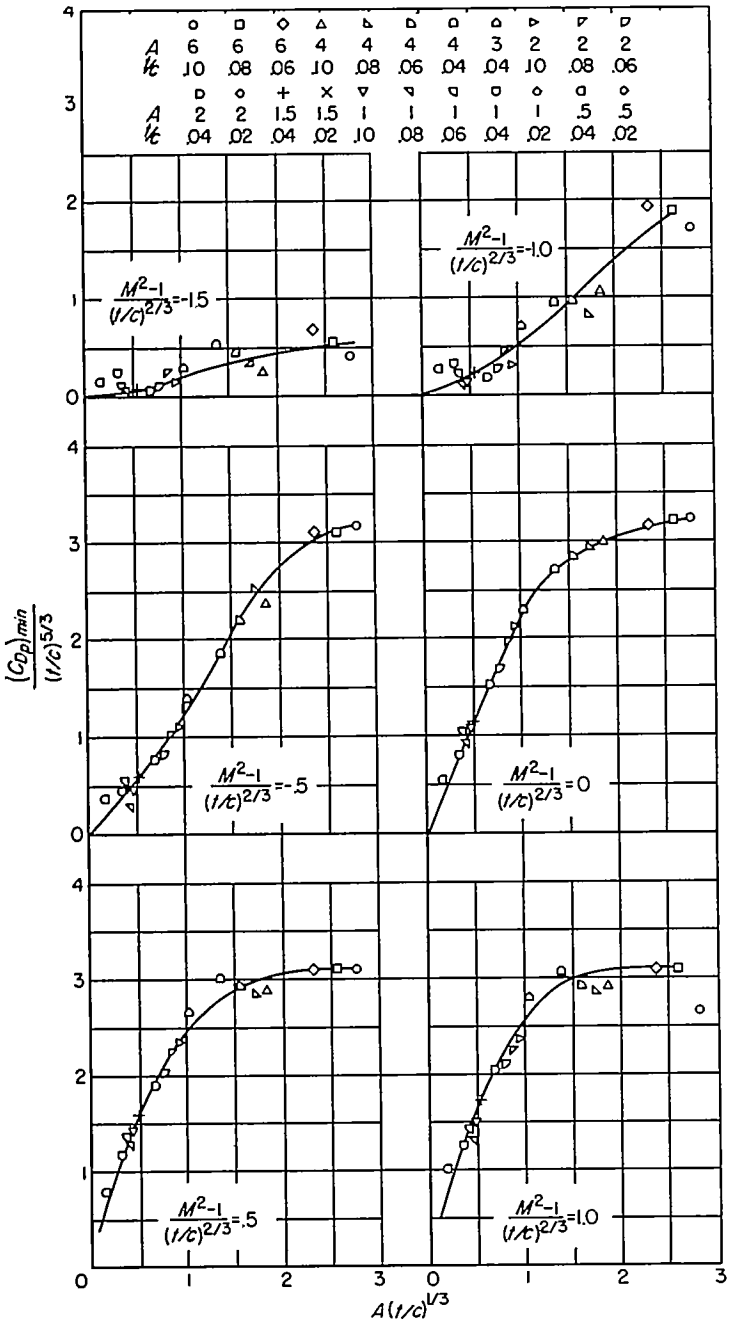

FIGURE 6.—The correlation of minimum pressure drag for the symmetrical wings.

$$\frac{(C_{D_p})_{min}}{(t/c)^{5/3}}=\mathcal{D}p\left[\frac{M^2-1}{(t/c)^{2/3}}, A\left(\frac{t}{c}\right)^{1/3}\right] \tag{15}$$

where the minimum pressure drag coefficient was obtained by subtracting a constant friction drag coefficient (assumed equal to the minimum drag coefficient at 0.7 Mach number) from the minimum drag coefficient; that is,

$$(C_{D_p})_{min}=C_{D_{min}}-(C_{D_{min}})_{M=0.7} \tag{16}$$

The data for the 2-percent-thick wing models were omitted from figure 6 because of the uncertainty of reading accurately the rather small transonic drag rise of these models. These thinnest airfoils had unusually large value of $\frac{(C_{D_p})_{min}}{(t/c)^{5/3}}$ which might be the result of the boundary layer creating an effective thickness considerably larger than the actual profile thickness. The generalized drag coefficients are then magnified for the thin airfoils by the 5/3 powers of the ratios of effective thickness to profile thickness.

Although the data correlation was poor in the vicinity of the critical Mach number [4] the correlation is remarkably

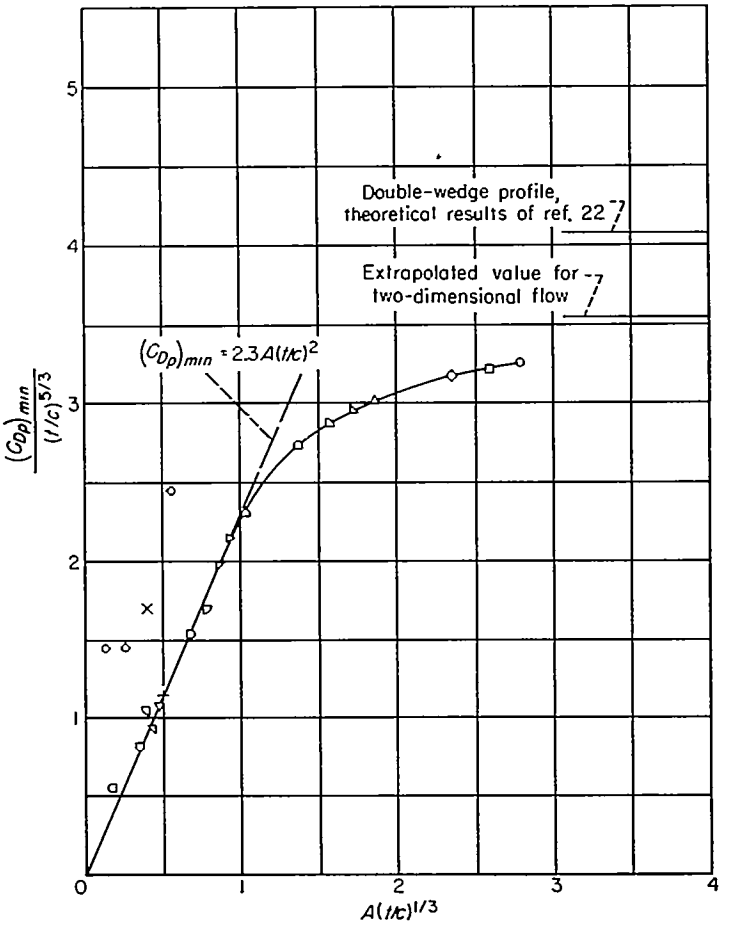

FIGURE 7.—The correlation of minimum pressure drag at $M=1$ for the symmetrical wings.

good at the sonic Mach number and the results for this Mach number are repeated in figure 7. (The data for 2-percent thickness are included in figure 7 to illustrate the pronounced effect of the boundary layer for these thinnest profiles.) At $M=1$ the minimum pressure drag coefficient is seen to vary linearly with aspect ratio and with the second power of the thickness ratio for values of $A(t/c)^{1/3}$ less than about 1,

$$\left.\begin{aligned}(C_{D_p})_{min}&=2.3A\left(\frac{t}{c}\right)^2, \qquad M=1\\ A\left(\frac{t}{c}\right)^{1/3}&<1\end{aligned}\right\} \tag{17}$$

[4] In reference 5 Kaplan has shown that the section critical Mach number, according to first-order linearized theory, is related to the thickness ratio by a constant value of the speed parameter, the constant depending on the particular profile shape. The predicted critical Mach numbers for NACA 630AXX profiles (ref. 21) may be approximated by

$$\frac{M_{cr}^2-1}{(t/c)^{2/3}}=-1.95$$

For values of $A(t/c)^{1/3}$ greater than 1 the generalized coefficient $\frac{(C_{D_p})_{min}}{(t/c)^{5/3}}$ approaches rapidly and asymptotically a constant value for which the minimum pressure drag coefficient varies with the 5/3 power of the thickness ratio in accordance with the drag similarity rule for sonic, two-dimensional flow. The extrapolated two-dimensional-flow value for $M=1$, $(C_{D_p})_{min}=3.55(t/c)^{5/3}$, was obtained by plotting against the inverse parameter $\frac{1}{A(t/c)^{1/3}}$. The theoretical pressure drag coefficient for a double-wedge profile (ref. 22) is somewhat higher.

The correlation of minimum pressure drag is summarized in figure 8 by cross-plotting from the faired curves of figure 6.

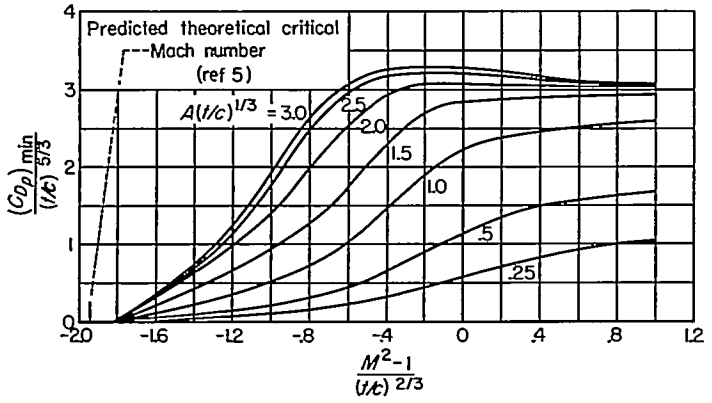

FIGURE 8.—Summary curves of the generalized minimum pressure drag coefficient for the symmetrical wings.

The fundamental importance of the similarity parameter $A(t/c)^{1/3}$ is clearly evident from the preceding correlation. A further indication of the importance of this parameter can be obtained from a comparison of figures 5 and 8 which illustrates how a multiple family of basic data curves can be summarized by a single presentation involving only one geometric parameter.

Drag due to lift.—The drag-due-to-lift parameter $\Delta C_D/C_L^2$ is difficult to correlate because of the many factors involved. In addition to changes in flow separation and in boundary-layer development with changing angle of attack, there are other factors such as shock-wave interaction with the boundary layer that lead to departure of the drag polars from the parabolic shape. However, for small values of lift coefficient, the drag due to lift may be assumed to vary linearly with C_L^2 and the following similarity rule results

$$\left.\begin{aligned}\left(\frac{t}{c}\right)^{-1/3}\frac{\Delta C_D}{C_L^2}&=\Delta\mathcal{D}_1\left[\frac{M^2-1}{(t/c)^{2/3}},A\left(\frac{t}{c}\right)^{1/3}\right]\\ \Delta C_D&\sim C_L^2\\ C_L&\sim\alpha\end{aligned}\right\} \tag{18}$$

The basic data curves showing the variation of $\Delta C_D/C_L^2$ with Mach number are presented in figure 9 and the correlation of these data is shown in figure 10. The dashed lines of figure 10 represent the idealized limits for drag due to lift with full leading-edge suction and with no leading-edge suction. The theoretical drag due to lift with full leading-

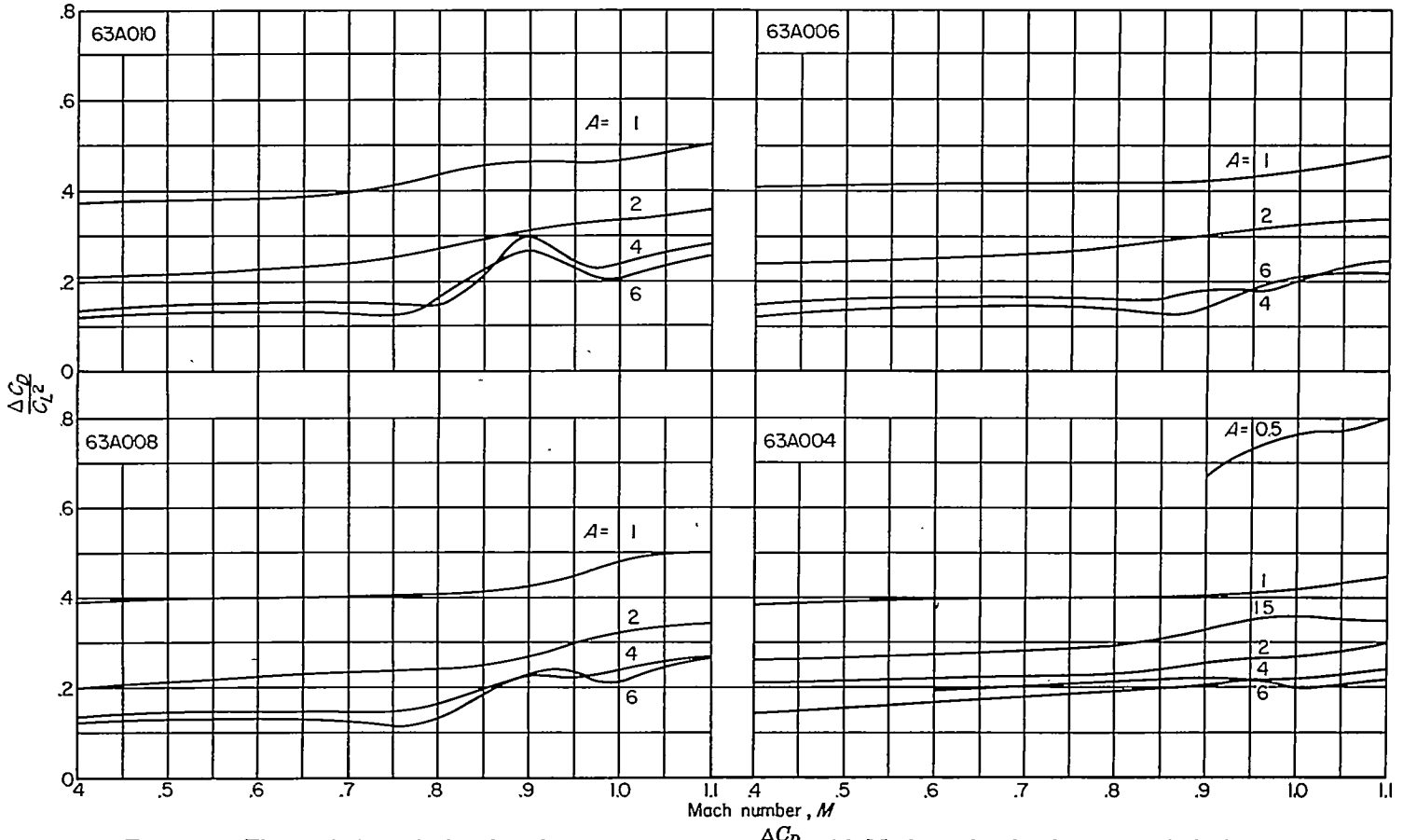

FIGURE 9.—The variation of the drag-due-to-lift parameter $\frac{\Delta C_D}{C_L^2}$ with Mach number for the symmetrical wings.

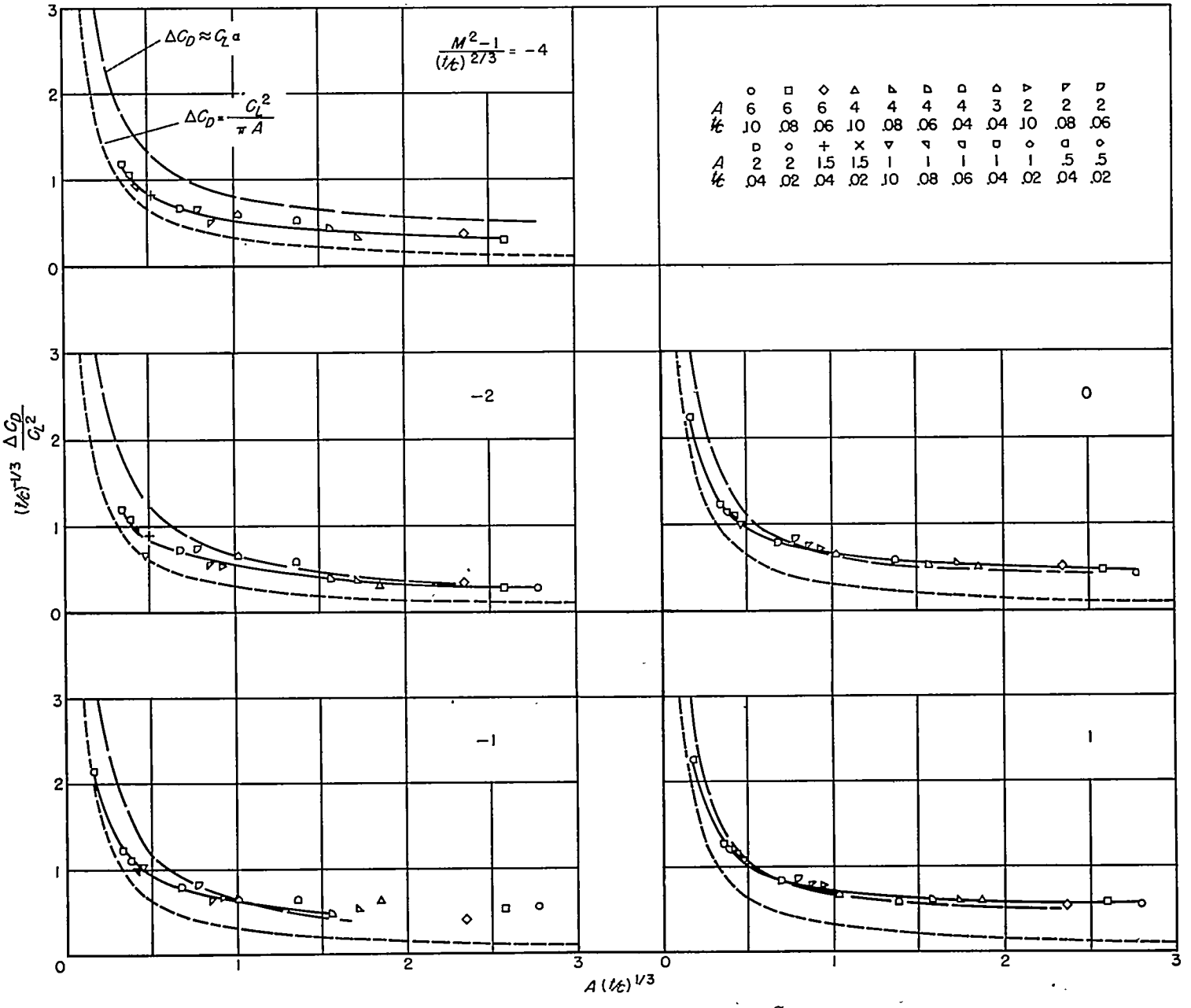

FIGURE 10.—The correlation of the drag-due-to-lift parameter, $(t/c)^{-1/3} \frac{\Delta C_D}{C_L^2}$, for the symmetrical wings.

edge suction is (when an elliptical spanwise variation of loading is assumed)

$$\Delta C_D = \frac{C_L^2}{\pi A} \tag{19}$$

and for no leading-edge suction (resultant force perpendicular to the plane of the wing) the following approximate relationship can be used:

$$\Delta C_D \approx C_L \alpha \tag{20}$$

In terms of the similarity parameters these equations become

$$\left(\frac{t}{c}\right)^{-1/3} \frac{\Delta C_D}{C_L^2} = \frac{1}{\pi A (t/c)^{1/3}} \tag{21}$$

$$\left(\frac{t}{c}\right)^{-1/3} \frac{\Delta C_D}{C_L^2} \approx \frac{1}{(t/c)^{1/3} dC_L/d\alpha} \tag{22}$$

Numerical values for $(t/c)^{1/3}(dC_L/d\alpha)$ are presented in figure 3. At subcritical speeds the data lie somewhere between the two limits; however, a gradual loss of leading-edge suction occurs when the wings enter the transonic speed range. At transonic speeds the drag force for the larger aspect ratios and thickness ratios is actually somewhat higher than the value corresponding to a resultant force perpendicular to the plane of the wing, suggesting that some increase in separation and viscous effects occurs with increasing angle of attack. A poor correlation was obtained for large values of $A(t/c)^{1/3}$ for values of the speed parameter near −1 where a poor correlation was also obtained with the lift data.

The parameter $(t/c)^{-1/3}(\Delta C_D/C_L^2)$ is inadequate for displaying drag-due-to-lift characteristics for small aspect ratios since this parameter becomes infinitely large as the aspect ratio goes to zero. An alternative similarity rule (obtained

by multiplying both sides of equation (18) by $A(t/c)^{1/3}$ which is suitable for low aspect ratios (but not for large aspect ratios) is the following: [5]

$$\left.\begin{aligned} A\frac{\Delta C_D}{C_L^2}&=\Delta\mathcal{D}_2\left[\frac{M^2-1}{(t/c)^{2/3}}, A\left(\frac{t}{c}\right)^{1/3}\right]\\ C_L&\sim\alpha\\ \Delta C_D&\sim C_L^2 \end{aligned}\right\} \tag{23}$$

The $M=1$ data are presented in figure 11 in the manner suggested by equation (23). Only for very low values of $A(t/c)^{1/3}$ does the drag due to lift tend toward the formal result of slender-wing theory $\Delta C_D=(\pi/4)A\alpha^2$. As a result of the gradual loss of leading-edge suction as $A(t/c)^{1/3}$ varies from 0 to 1, the experimental data in the similarity scheme can be approximated by a straight line which leads to the empirical relationship

$$\frac{\Delta C_D}{C_L^2}=\frac{1}{\pi A}+0.35\left(\frac{t}{c}\right)^{1/3} \tag{24}$$

The drag-due-to-lift correlation is summarized in figure 12 by cross-plotting the faired curves of figure 10.

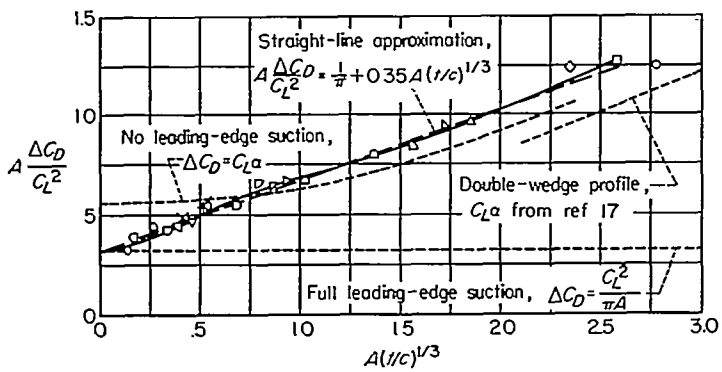

FIGURE 11.—The correlation of the drag-due-to-lift parameter $A\frac{\Delta C_D}{C_L^2}$ at $M=1$ for the symmetrical wings.

[5] A parameter suitable for displaying simultaneously the drag-due-to-lift behavior for small values of $A(t/c)^{1/3}$ and the asymptotic behavior for large $A(t/c)^{1/3}$ is the parameter $(t/c)^{1/3}(\Delta C_D/\alpha^2)$. (See fig. 16 of ref. 8.) It is more instructive, however, to use the ratio of the drag due to lift to the lift coefficient squared as in the present report.

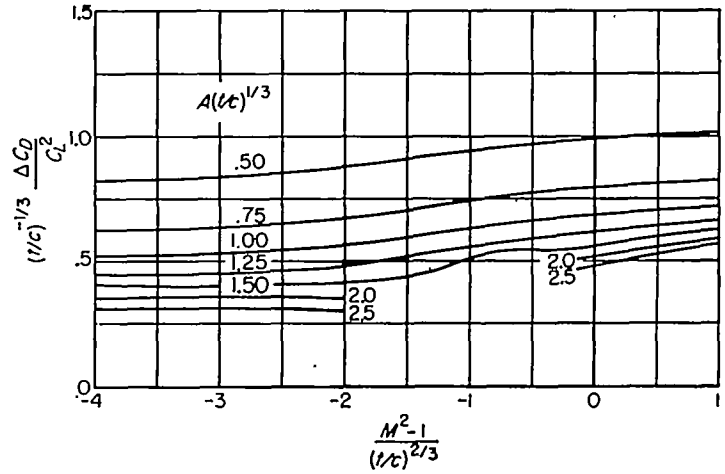

FIGURE 12.—Summary curves of the generalized drag-due-to-lift parameter, $(t/c)^{-1/3}\frac{\Delta C_D}{C_L^2}$, for the symmetrical wings.

MOMENT

The similarity rule for pitching-moment-curve slope is

$$\frac{dC_m}{dC_L}=\mathcal{M}\left[\frac{M^2-1}{(t/c)^{2/3}}, A\left(\frac{t}{c}\right)^{1/3}, \frac{\alpha}{t/c}\right] \tag{25}$$

where it is necessary to include the parameter $\frac{\alpha}{t/c}$ since the data is often nonlinear, especially for wings of small aspect ratio.

The variation of dC_m/dC_L with Mach number for $\frac{\alpha}{t/c}$ ratios of 0, 1, and 2 radians is presented in figure 13. (The values of α in degrees are tabulated in table III.) For the larger aspect ratios dC_m/dC_L behaves erratically at high subsonic speeds, the erratic behavior probably being due to the same causes as the irregularities of the lift-curve slope and drag due to lift at the corresponding Mach numbers. At Mach numbers up to the critical, the effects of compressibility are relatively small as is predicted by linearized theory. At transonic speeds a large change in the center of pressure occurs for the wings of large aspect ratio, the aerodynamic center moving from the vicinity of the 25-percent chord at subsonic speeds toward the midchord at supersonic speeds. Only for very low aspect ratios is this change in center of pressure substantially decreased.

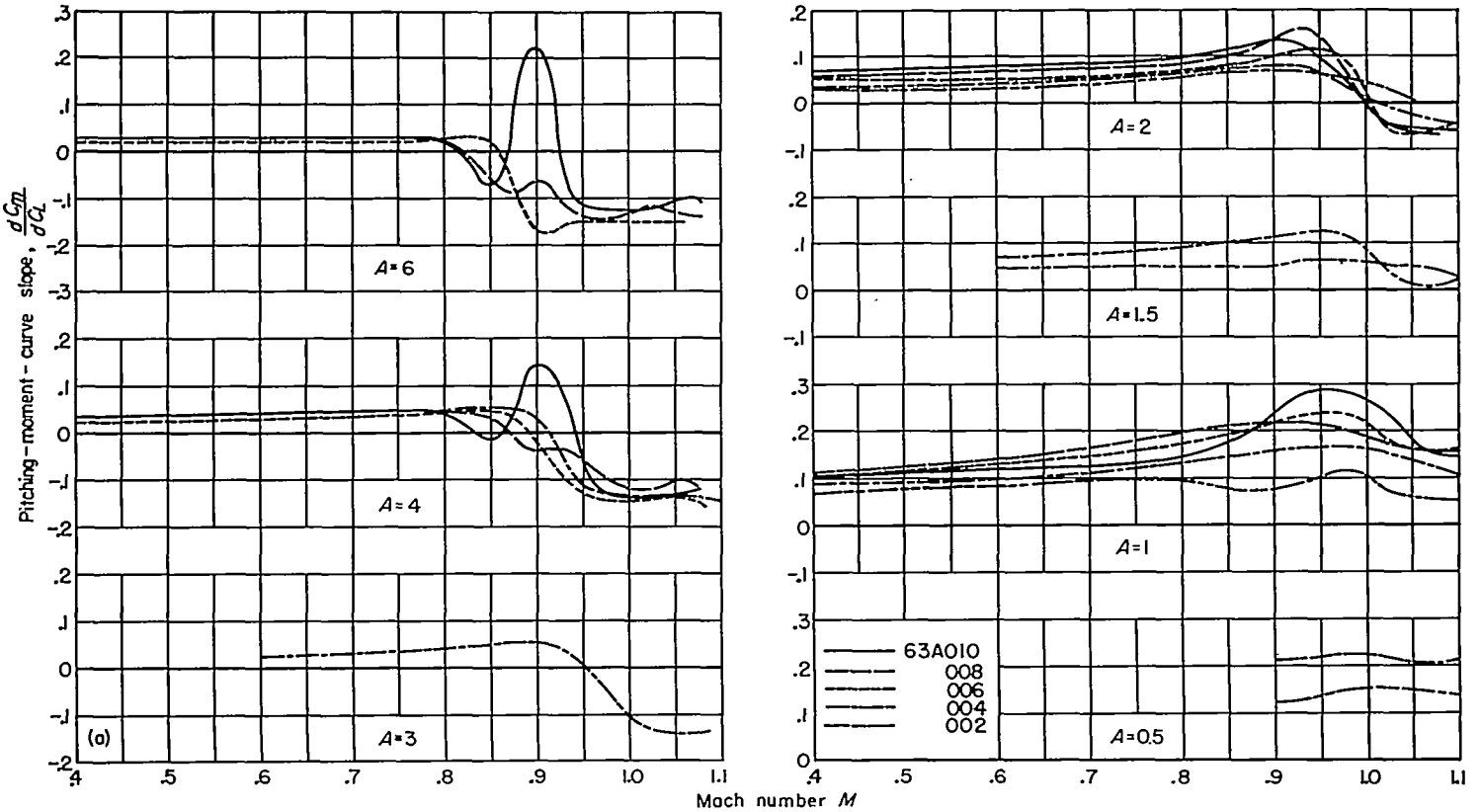

(a) $\frac{\alpha}{t/c}$, 0

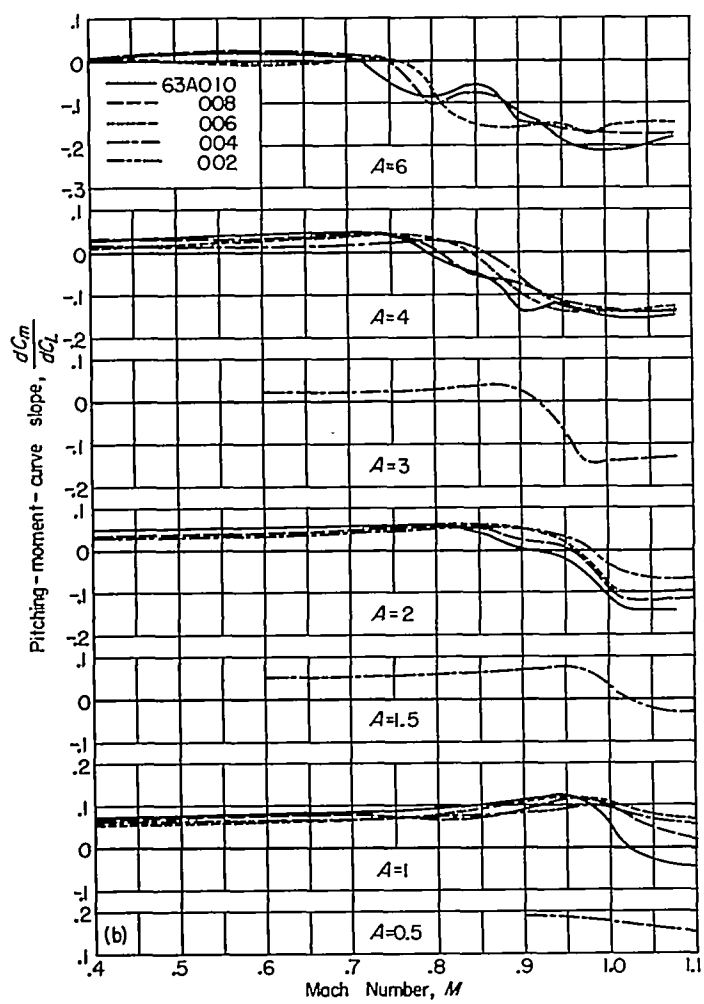

(b) $\frac{\alpha}{t/c}$, 1

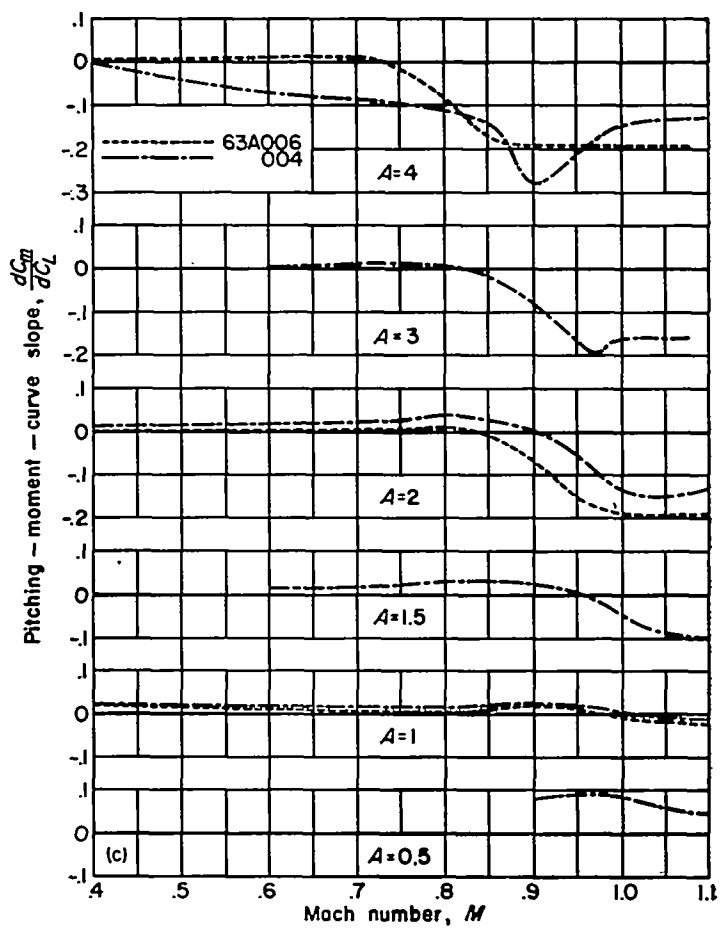

(c) $\frac{\alpha}{t/c}$, 2

FIGURE 13.—The variation of pitching-moment-curve slope with Mach number for the symmetrical wings.

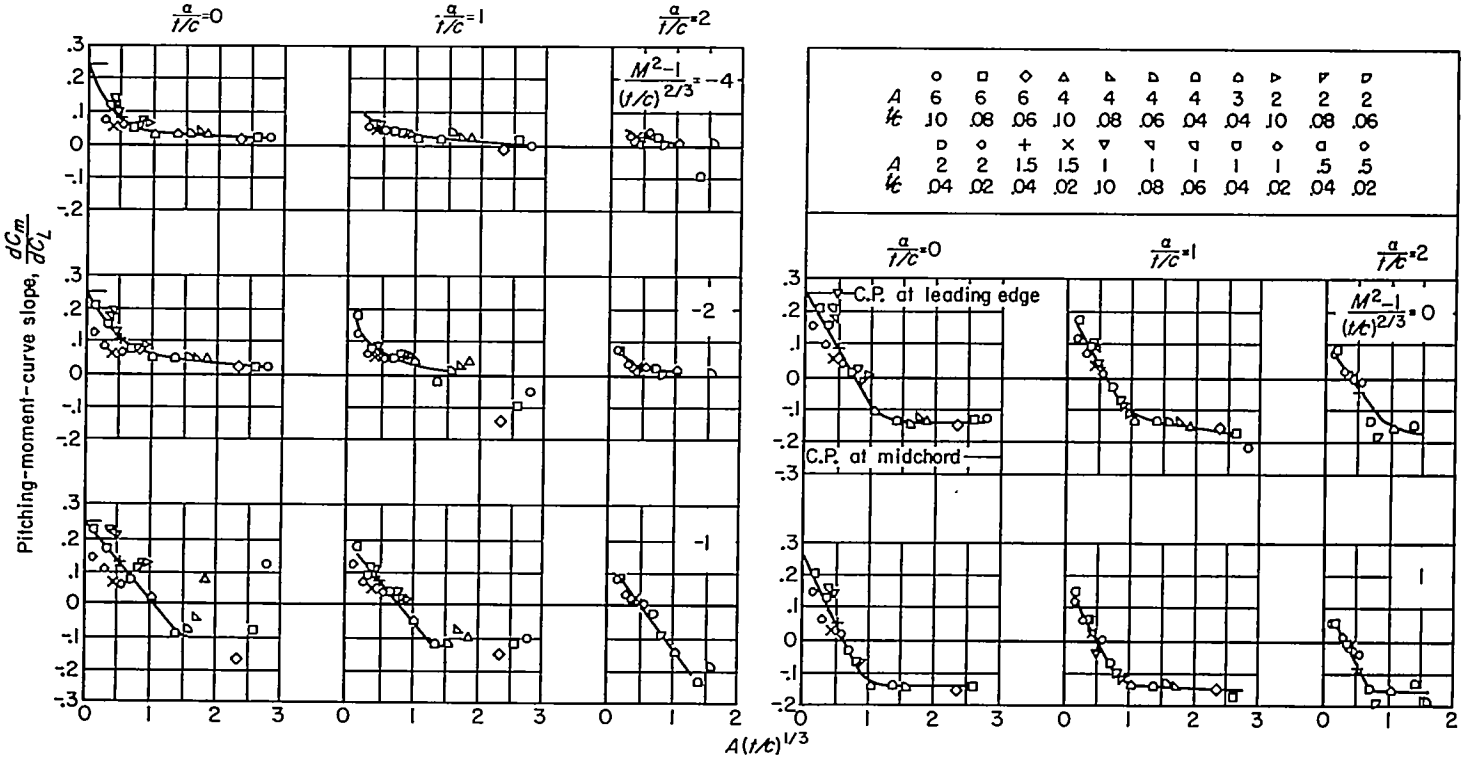

FIGURE 14.—The correlation of pitching-moment-curve slope for the symmetrical wings.

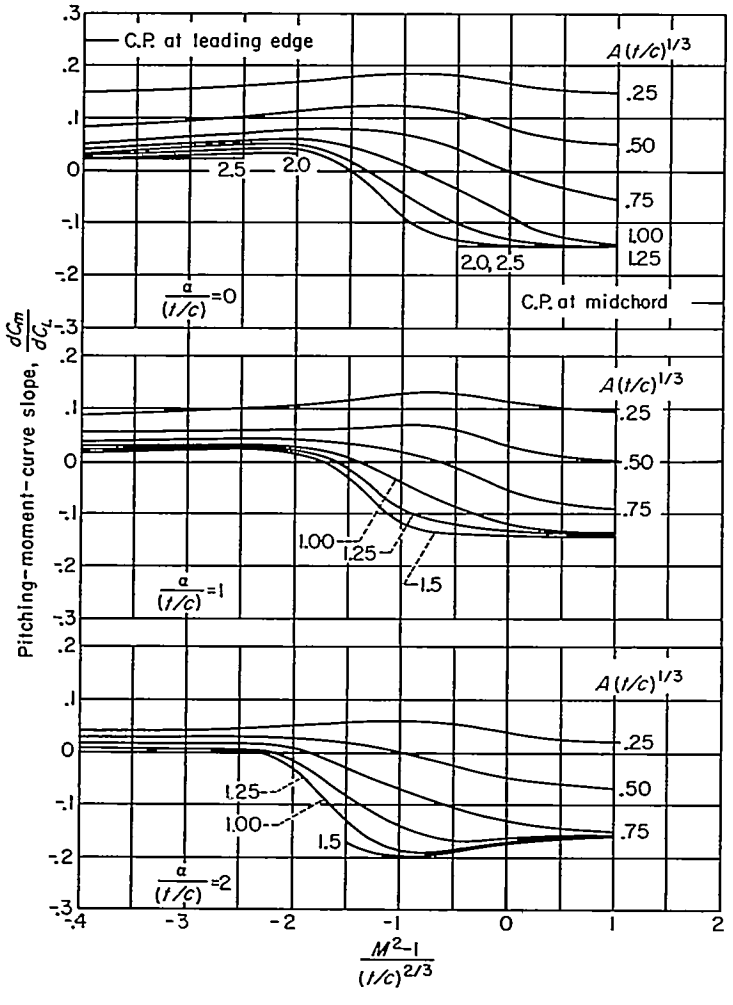

FIGURE 15.—Summary curves for pitching-moment-curve slope for the symmetrical wings.

The correlation of dC_m/dC_L is presented in figure 14. Although considerable scatter of data is evident, the curves have been faired to favor the data for thickness ratios of 4 percent which do show a good correlation. The values of dC_m/dC_L for $\frac{\alpha}{t/c}=0$ represent the position of the center of pressure for zero lift and, for all values of the speed parameter, the center of pressure is shown to move progressively toward the leading edge as the aspect ratio approaches zero, a result to be expected from a consideration of slender-wing theory. At $M=1$ a linear variation of dC_m/dC_L with $A(t/c)^{1/3}$ is a reasonable approximation for values of $A(t/c)^{1/3}$ less than about 1 while for values greater than 1 the pitching-moment-curve slope may be considered to be constant and independent of both aspect ratio and thickness ratio. The correlation is summarized in figure 15 by cross-plotting the faired curves of figure 14.

MAXIMUM LIFT-DRAG RATIO AND OPTIMUM LIFT COEFFICIENT

The maximum lift-drag ratio and the optimum lift coefficient are given by the following formulas when the drag polars are parabolic:

$$\left(\frac{L}{D}\right)_{max}=\frac{1}{2}\sqrt{\frac{1}{[C_{D_f}+(C_{D_p})_{min}]\frac{\Delta C_D}{C_L^2}}} \tag{26}$$

$$C_{L_{opt}}=\sqrt{\frac{C_{D_f}+(C_{D_p})_{min}}{\frac{\Delta C_D}{C_L^2}}} \tag{27}$$

Because of the friction drag, generalized expressions in terms of the similarity parameters are not useful in correlating

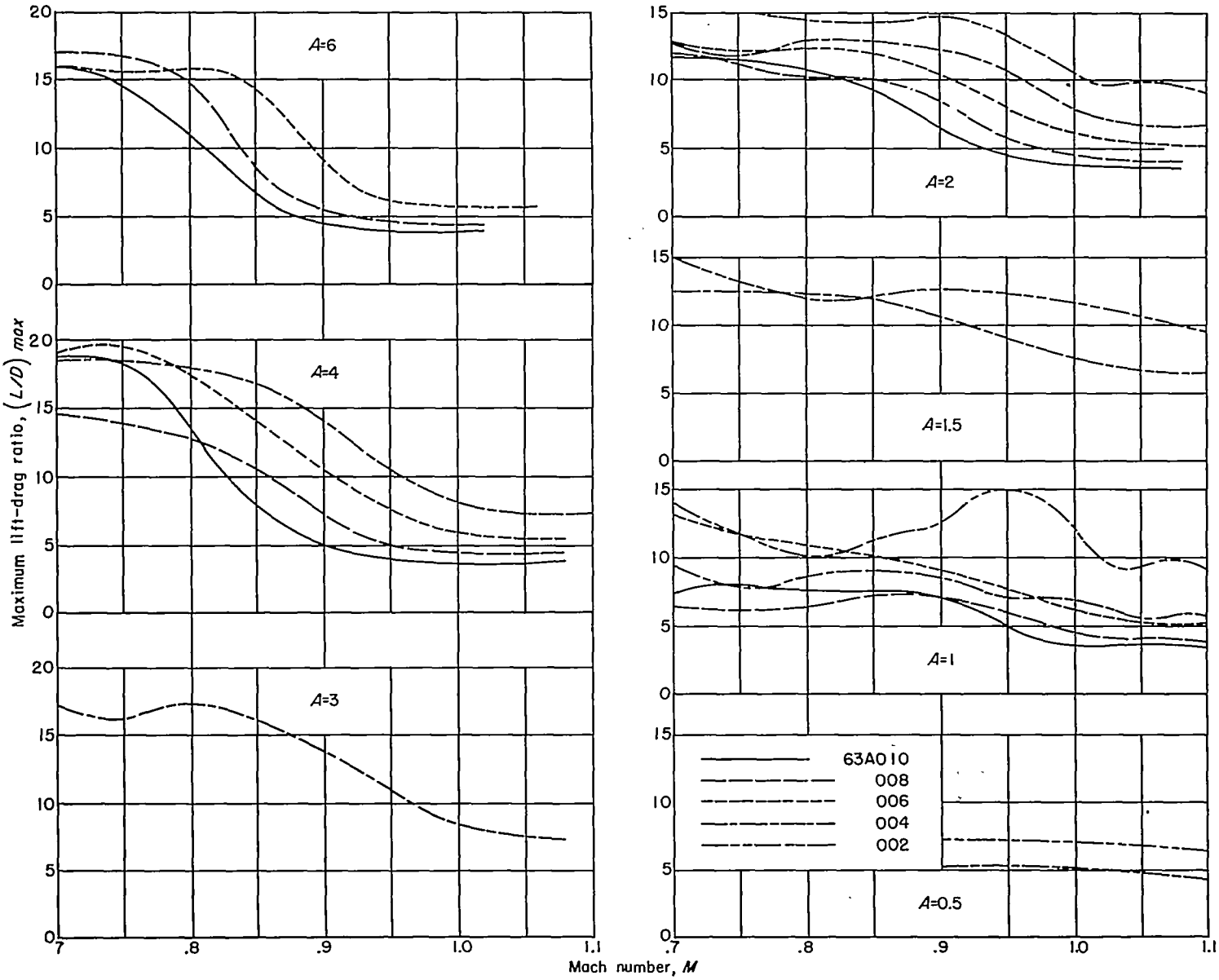

FIGURE 16.—The variation of maximum lift-drag ratio with Mach number for the symmetrical wings.

experimental data. However, a few remarks will be made concerning the effects of aspect ratio and thickness ratio at transonic speeds.

The variation of $(L/D)_{max}$ with Mach number is presented in figure 16. At low speeds and large Reynolds numbers, the maximum lift-drag ratio depends principally on the value of the aspect ratio. Above the critical Mach number, where the pressure drag becomes large, the lift-drag ratios are found to be essentially independent of aspect ratio but indicate a pronounced dependence on the thickness ratio. This independence of aspect ratio at transonic speeds is due largely to the opposite variations of drag due to lift and minimum drag with aspect ratio.

At $M=1$ the linear variation of force coefficients with aspect ratio is characteristic of wings having values of $A(t/c)^{1/3}$ less than about 1. The following formulas were obtained by use of the empirical relationships given by equations (17) and (24):

$$\left(\frac{L}{D}\right)_{max}=\frac{1}{2}\left\{\left[C_{D_f}+2.3A\left(\frac{t}{c}\right)^2\right]\left[\frac{A}{\pi}+0.35\left(\frac{t}{c}\right)^{1/3}\right]\right\}^{-1/2}, \quad \begin{matrix} M=1 \\ A\left(\frac{t}{c}\right)^{1/3}<1 \end{matrix} \tag{28}$$

$$C_{L_{opt}}=\sqrt{\frac{C_{D_f}+2.3A(t/c)^2}{\frac{A}{\pi}+0.35(t/c)^{1/3}}}, \quad \begin{matrix} M=1 \\ A\left(\frac{t}{c}\right)^{1/3}<1 \end{matrix} \tag{29}$$

A comparison of maximum lift-drag ratios according to equation (28), assuming that $C_{D_f}=0.0070$, with experimental data is made in figure 17.

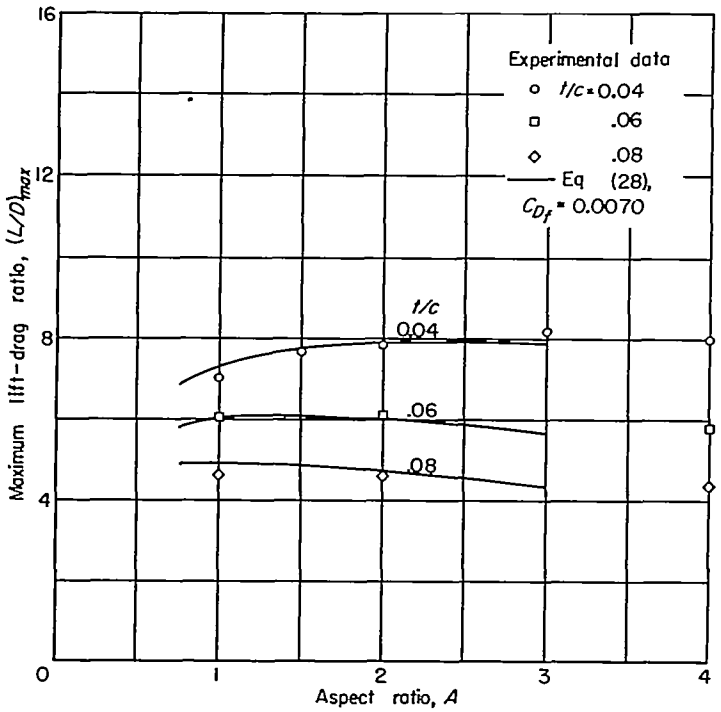

FIGURE 17.—Maximum lift-drag ratios at $M=1$ for the symmetrical wings.

II. CAMBERED PROFILES

The cambered wings have been grouped into families according to the value of the camber-to-thickness ratio h/t in order that the transonic similarity rules can be used in the data analysis. The camber parameter h represents the amount of camber and is defined as the maximum displacement of the mean line from the chord line (see fig. 18).

The cambered wings chosen for the data correlation belong in one of three basic families for which the camber-to-thickness ratios, h/t, are 0.222, 0.333, and 0.444. These airfoils are listed in the following table:

h/t	NACA profile	t/c	h/c	Aspect ratios
0.222	63A206	0.06	0.0133	4, 3, 2, 1.5, 1
.333	63A204	.04	.0133	4, 3, 2, 1.5, 1
	63A408	.08	.0266	4, 2, 1
.444	63A406	.06	.0266	4, 3, 2, 1.5, 1

Some of the results of the previous data correlation for the symmetrical wings ($h/t=0$) are repeated here in order to form a basis for determining the effects of this type of camber on the transonic characteristics of rectangular wings.

LIFT

The lift correlation is presented as separate studies of the lift-curve slope and of the displacement of the lift curve due to the presence of camber. When a linear variation of C_L with α is assumed, the following generalized expression for the lift-curve slopes of cambered wings results

$$\left.\begin{aligned}\left(\frac{t}{c}\right)^{1/3}\frac{dC_L}{d\alpha}&=\mathcal{L}_1\left[\frac{M^2-1}{(t/c)^{2/3}},A\left(\frac{t}{c}\right)^{1/3},\frac{h}{t}\right]\\ C_L&\sim\alpha\end{aligned}\right\} \tag{30}$$

The displacement of the lift curve can be studied by use of either the generalized expression for the angle of attack for zero lift

$$\frac{\alpha_0}{h/c}=\mathcal{L}_2\left[\frac{M^2-1}{(t/c)^{2/3}},A\left(\frac{t}{c}\right)^{1/3},\frac{h}{t}\right] \tag{31}$$

or the generalized expression for the lift coefficient at zero angle of attack

$$\left(\frac{t}{c}\right)^{1/3}\frac{(C_L)_{\alpha=0}}{h/c}=\mathcal{L}_3\left[\frac{M^2-1}{(t/c)^{2/3}},A\left(\frac{t}{c}\right)^{1/3},\frac{h}{t}\right] \tag{32}$$

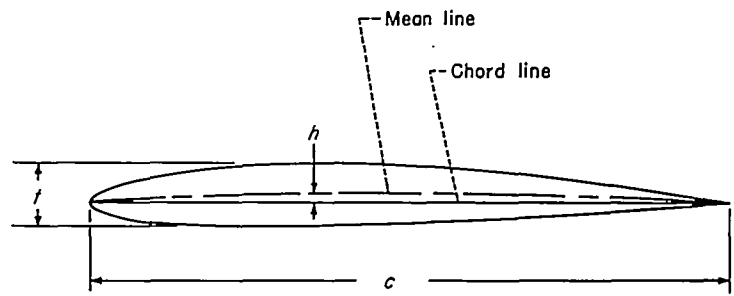

FIGURE 18.—Wing-profile nomenclature.

Since the latter two equations are related to each other by virtue of the generalized lift-curve slope (eq. (30)), it is sufficient to consider only one of these equations.

Angle of attack for zero lift.—The correlation of the angle of attack for zero lift is presented in figure 19. It should be recognized that the angle of attack for zero lift is particularly sensitive to model construction details, tunnel flow characteristics, and accuracy of measurements, making this a difficult parameter to correlate.

Since the parameter $\frac{\alpha_0}{h/c}$ did not show a systematic dependence on the value of the camber-to-thickness ratio h/t, all the wings of the various camber-to-thickness families have been grouped together in the correlation and a single curve has been drawn through the data points. For Mach numbers less than the critical $\left(\text{which is in the neighborhood of } \frac{M^2-1}{(t/c)^{2/3}}=-2\right)$ the angle of attack for zero lift shows little change with changes in Mach number, and the experimental values of α_0 for wings of large aspect ratio are closely predicted by two-dimensional flow theory.[6] When the critical Mach number is exceeded, the changes occurring with increasing Mach number are quite large for all but the very low aspect ratios which are characteristically insensitive to changes in Mach number. Upon entering the transonic speed range the wings of large aspect ratio lost most of the camber effect, a result to be expected since, according to linearized supersonic flow theory, the addition of camber does not affect the lift.

[6] The theoretical value shown in figure 19 was calculated by use of the $\alpha=0.8$ (modified) mean-line data of figure 3, reference 14, and equation (16) of reference 21.

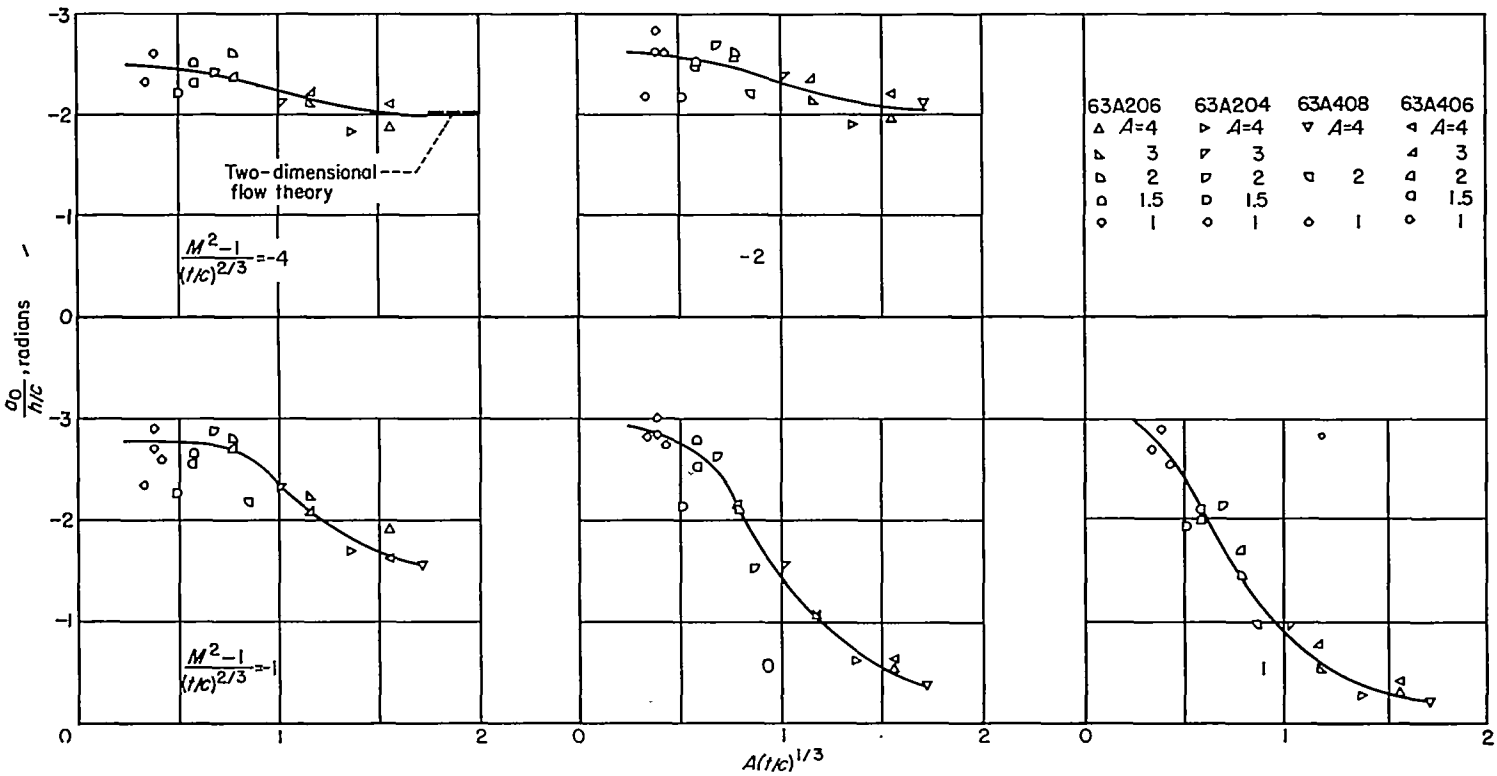

FIGURE 19.—The correlation of angle of attack for zero lift for the cambered wings.

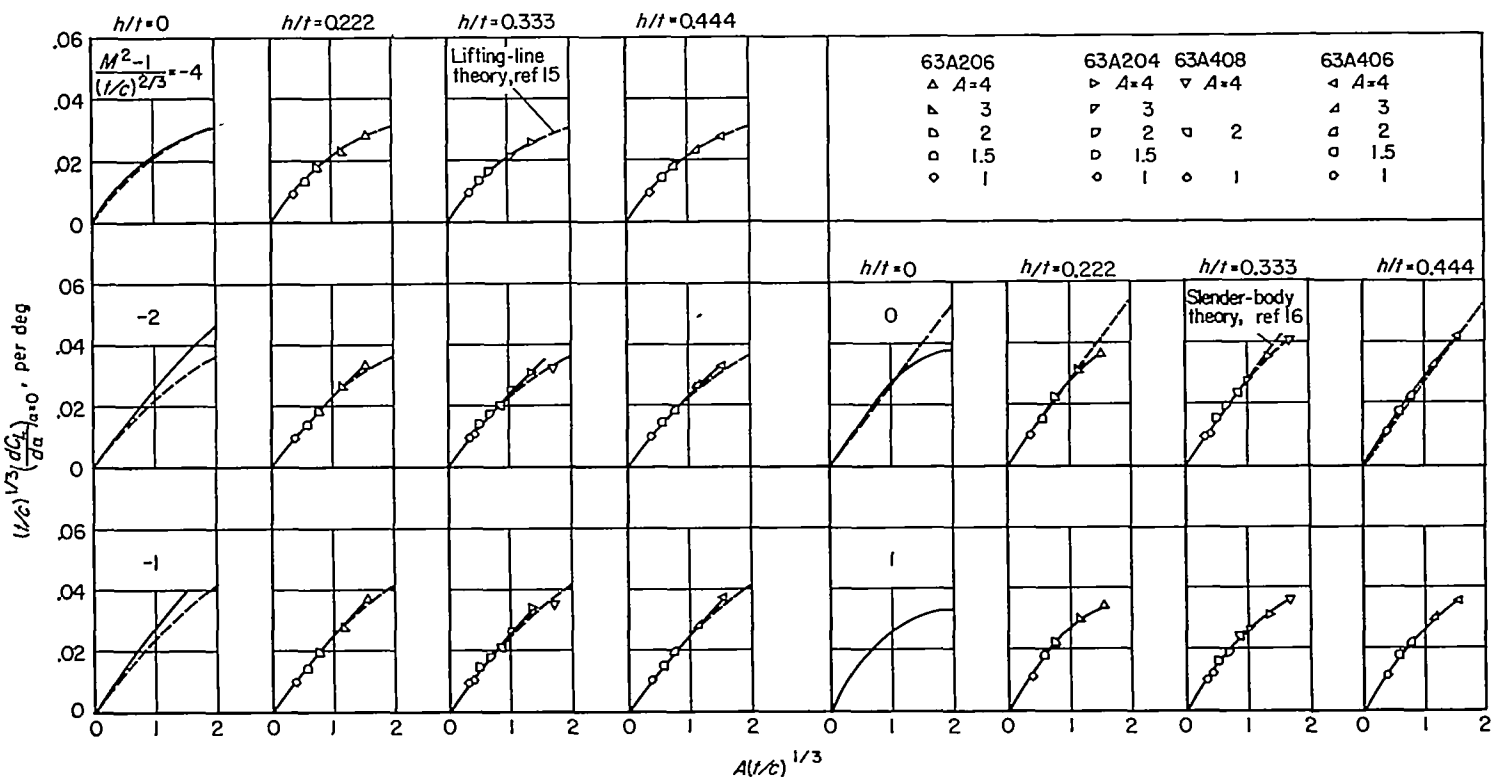

FIGURE 20.—The correlation of lift-curve slope for the cambered wings.

Lift-curve slope.—The correlation of lift-curve slope is presented in figure 20 with each camber-to-thickness-ratio family presented separately since the lift-curve slope appeared to depend on the camber-to-thickness ratio at transonic speeds for large values of $A(t/c)^{1/3}$. The experimental data for subsonic speeds are compared with the Weissinger lifting-line theory (ref. 15), and at $M=1$ a comparison is made with slender-body theory (ref. 16).

Camber apparently has no appreciable effect on lift-curve slope (measured at zero angle of attack) at subcritical speeds nor at transonic speeds for wings of low aspect ratio ($A(t/c)^{1/3}$ less than about 1). At transonic speeds the lift-curve slope for wings of large aspect ratio appears to increase with increasing h/t.

DRAG

When a wing is cambered, it is difficult to separate the drag into components according to equation (13); in particular, it is difficult to ascertain a minimum-pressure drag which is free from induced-drag effects. A drag analysis of cambered-wing data is complicated further by the large changes in viscous effects which may occur as the lift changes from positive to negative. These viscous effects must be separated from the pressure drag if the transonic similarity rule is to be applied. One way, which is based on a number of approximations, to separate the viscous effects from the pressure drag is the following:

Linear variations of C_D with C_L^2 and C_L with α are assumed and the drag data at very small and at large lift coefficients are ignored. The drag components are then defined according to figure 21.

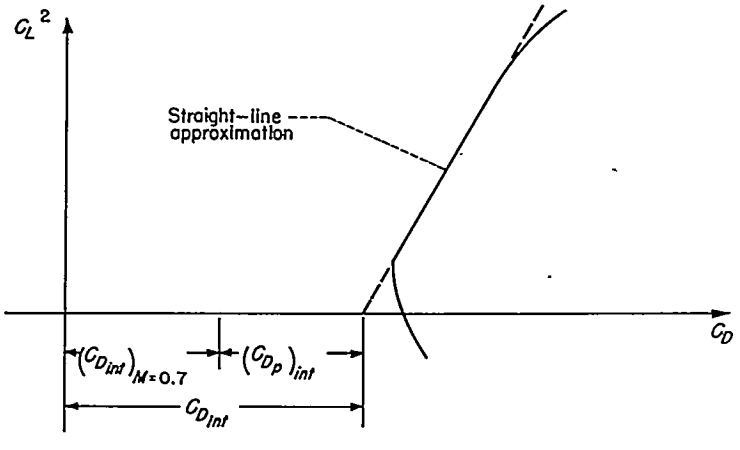

FIGURE 21.—Drag nomenclature for cambered wings.

A straight line is drawn as far as possible through the C_D versus C_L^2 data points and the intercept of this straight line with the zero-lift axis is then used to define an intercept drag coefficient $C_{D_{int}}$. The intercept pressure drag is defined as

$$(C_{D_p})_{int}=C_{D_{int}}-(C_{D_{int}})_{M=0.7} \tag{33}$$

and the slope of the straight-line approximation $\Delta C_D/C_L^2$ is used as a measure of the drag due to lift. The intercept drag coefficient $C_{D_{int}}$, as defined here, is a fictitious minimum drag coefficient and the actual minimum drag coefficient is somewhat higher. (The subcritical intercept drag for cambered wings may be thought of as corresponding to the friction drag of symmetrical wings.)

Intercept pressure drag.—The intercept pressure drag, equation (33), can be correlated by use of the similarity rule

$$\frac{(C_{D_p})_{int}}{(t/c)^{5/3}}=\mathcal{D}\left[\frac{M^2-1}{(t/c)^{2/3}}, A\left(\frac{t}{c}\right)^{1/3}, \frac{h}{t}\right] \tag{34}$$

The correlation is presented in figure 22 and compared with the previous results (dashed lines) for the symmetrical wings. The correlation indicates that the intercept pressure drag increases smoothly with increasing camber-to-thickness ratio. For moderate aspect ratios the increase in drag coefficient is roughly proportional to the camber-to-thickness ratio squared. As the aspect ratio becomes very small the camber effect tends to disappear, while for very large aspect ratios the generalized coefficients $\frac{(C_{D_p})_{int}}{(t/c)^{5/3}}$ apparently approach constant values which increase with increasing h/t. Data, however, were not available for sufficiently large aspect ratios to assess accurately the camber effect for two-dimensional flow.

Drag due to lift.—The drag-due-to-lift parameter $\Delta C_D/C_L^2$ is correlated in figure 23 according to the similarity rule

$$\left.\begin{aligned}\left(\frac{t}{c}\right)^{-1/3}\frac{\Delta C_D}{C_L^2}&=\Delta\mathcal{D}\left[\frac{M^2-1}{(t/c)^{2/3}}, A\left(\frac{t}{c}\right)^{1/3}, \frac{h}{t}\right]\\ C_L&\sim\alpha\\ \Delta C_D&\sim C_L^2\end{aligned}\right\} \tag{35}$$

The dashed curves in figure 23 represent the idealized limits for drag with full leading-edge suction, and drag with no leading-edge suction (see eqs. (21) and (22)). As evidenced by the correlation, the drag due to lift decreases consistently with increasing camber-to-thickness ratio throughout the entire Mach number range.

MOMENT

The pitching-moment characteristics are analyzed in two parts: the evaluation of pitching moment at zero angle of attack and the variation of pitching moment with angle of attack.

Pitching moment for zero angle of attack.—The correlation of pitching moment for zero angle of attack according to the similarity rule

$$\frac{(t/c)^{1/3}}{h/c}(C_m)_{\alpha=0}=\mathcal{M}_0\left[\frac{M^2-1}{(t/c)^{2/3}}, A\left(\frac{t}{c}\right)^{1/3}, \frac{h}{t}\right] \tag{36}$$

is presented in figure 24. The correlation parameter $\frac{(t/c)^{1/3}}{h/c}(C_m)_{\alpha=0}$ appears to be independent of the camber-to-thickness ratio h/t and, thus, the zero-angle-of-attack moment $(C_m)_{\alpha=0}$ can be considered to be linearly proportional to the camber ratio h/c throughout the speed range. The variation of $(C_m)_{\alpha=0}$ with changes in aspect ratio and Mach number is pronounced, in particular, the wings of large aspect ratio undergo substantial moment changes on entering the transonic speed range.

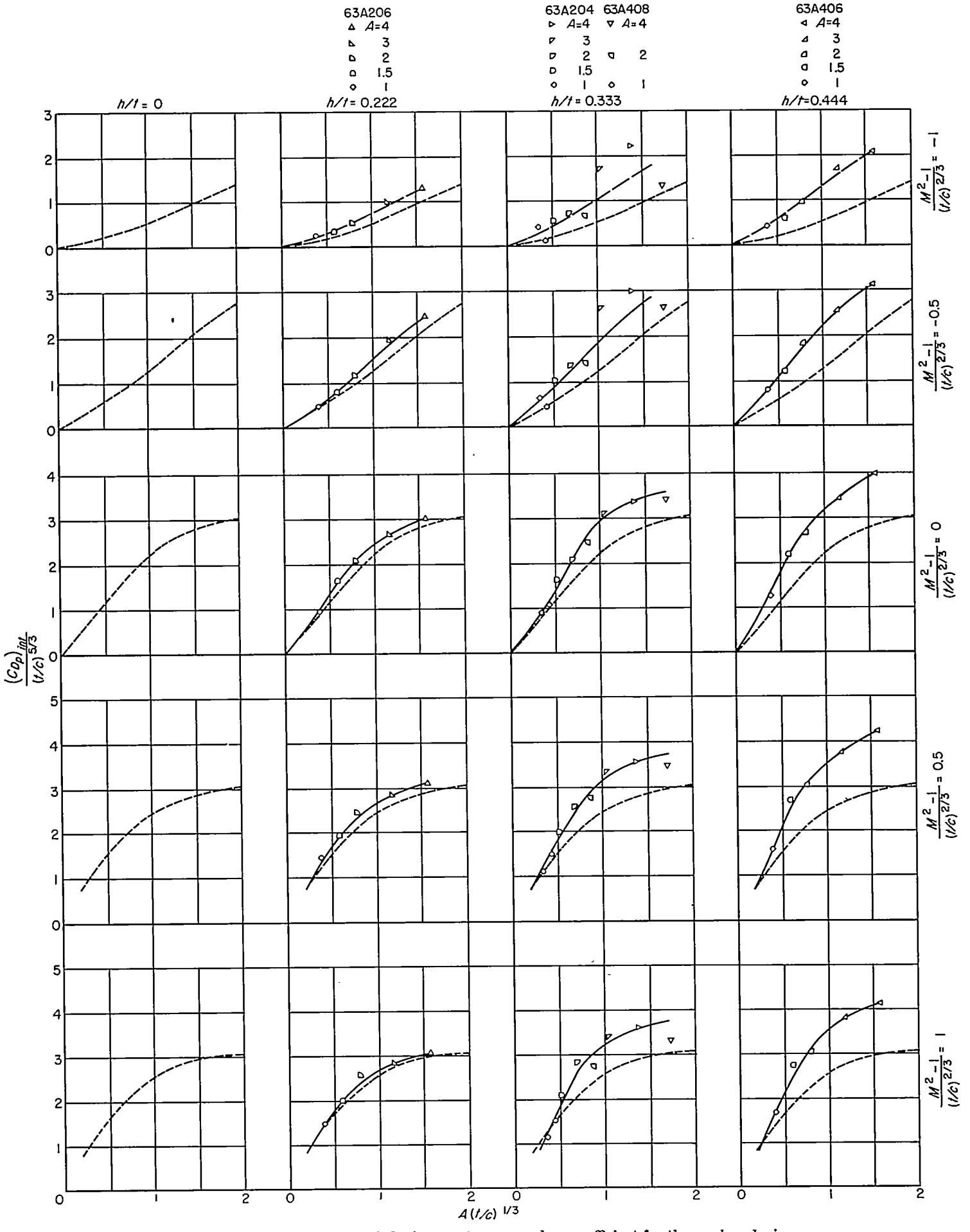

FIGURE 22.—The correlation of the intercept pressure-drag coefficient for the cambered wings.

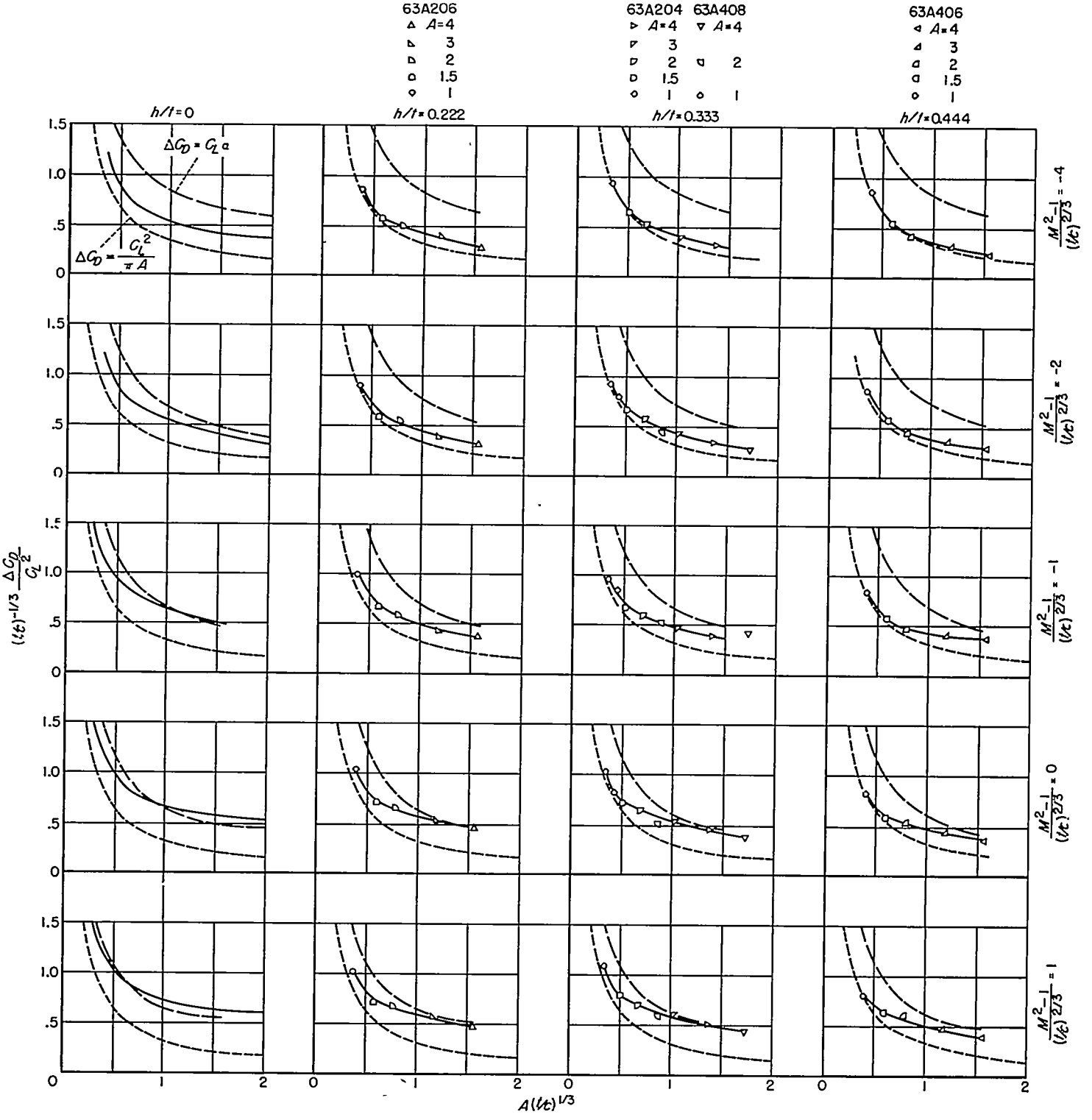

FIGURE 23.—The correlation of drag due to lift for the cambered wings.

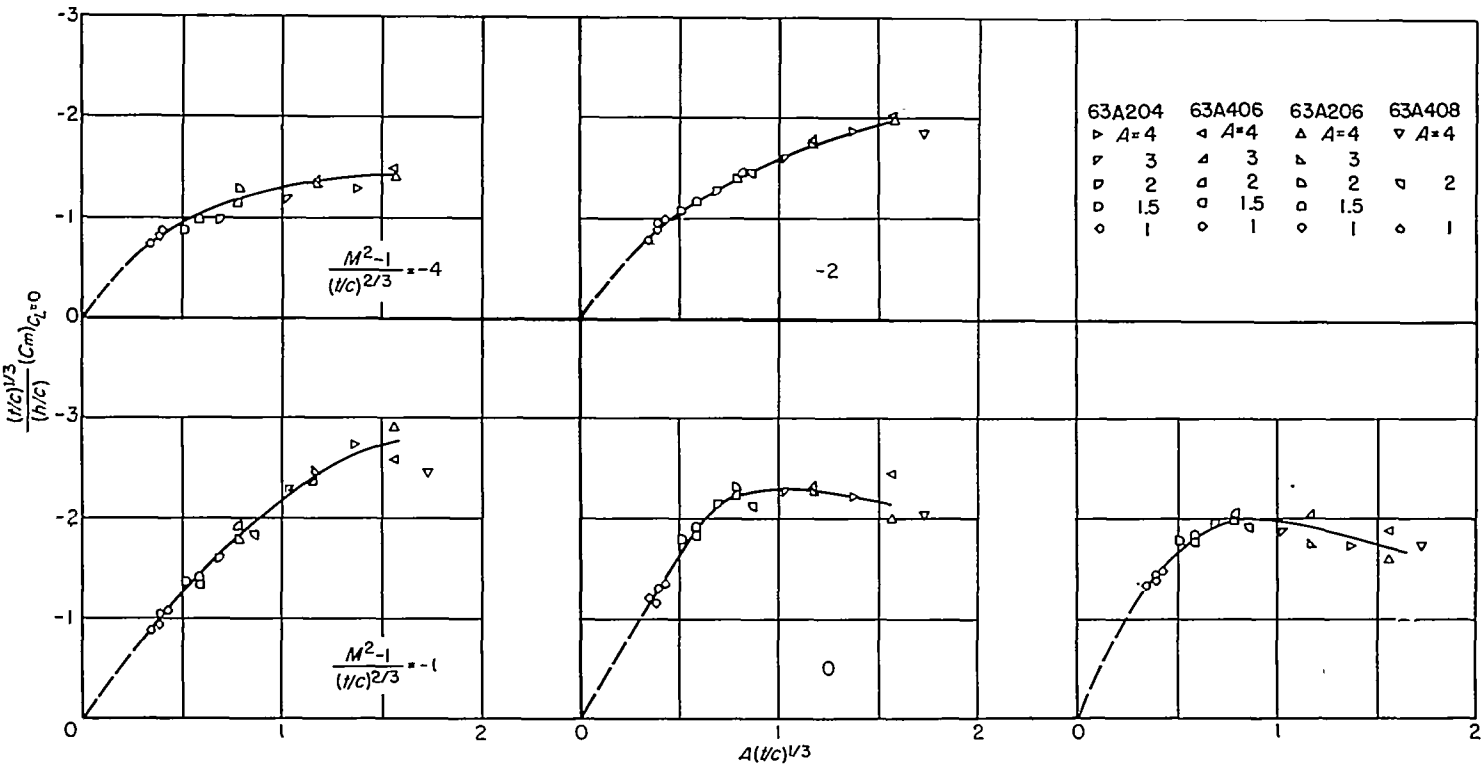

FIGURE 24.—The correlation of pitching-moment coefficient at zero lift for the cambered wings.

Pitching-moment-curve slope.—The moment-curve slope for cambered wings is expressed symbolically in the similarity scheme as

$$\frac{dC_m}{dC_L}=\mathcal{M}\left[\frac{M^2-1}{(t/c)^{2/3}}, A\left(\frac{t}{c}\right)^{1/3}, \frac{\alpha}{t/c}, \frac{h}{t}\right] \tag{37}$$

The correlation of dC_m/dC_L for $\frac{\alpha}{t/c}=0$ is presented in figure 25. For subcritical speeds and for values of $A(t/c)^{1/3}$ less than 1 the effect of camber is negligible. At transonic speeds for large values of $A(t/c)^{1/3}$ the addition of camber results in more negative values of dC_m/dC_L.

MAXIMUM LIFT-DRAG RATIOS

The correlated data at near sonic speeds indicates that the drag due to lift decreases somewhat as the intercept pressure drag increases. Because of the opposite effect of these two variations, it could be expected that L/D_{max} would not change greatly with changes in h/t. Although the similarity rule does not apply because of the friction drag, it is instructive to present the experimental maximum lift-drag-ratio data of reference 2 in terms of the camber-to-thickness ratio h/t. This has been done in figure 26 for the sonic value of the free-stream Mach number. For wings of moderately low aspect ratio (aspect ratios from about 1 to about 3), the effect of adding a small amount of camber is to increase slightly the maximum lift-drag ratio. It is difficult to say what value of h/t is optimum but, apparently (excluding the very thin wing, $t/c=0.02$, for which the boundary layer is a significant part of the wing effective thickness) the optimum occurs near $h/t=0.25$ with the most beneficial effect for aspect ratios near 2.

CONCLUDING REMARKS

This report shows that, with the exception of those wings of large $A(t/c)^{1/3}$ at high subsonic Mach numbers where erratic variations of force and moment coefficients occurred, it is possible to correlate experimental data for wings having a wide range of aspect ratios, thicknesses, and cambers by a unified method applicable at subsonic, transonic, and moderately supersonic Mach numbers. It is further demonstrated that, by proper use of the similarity parameters and

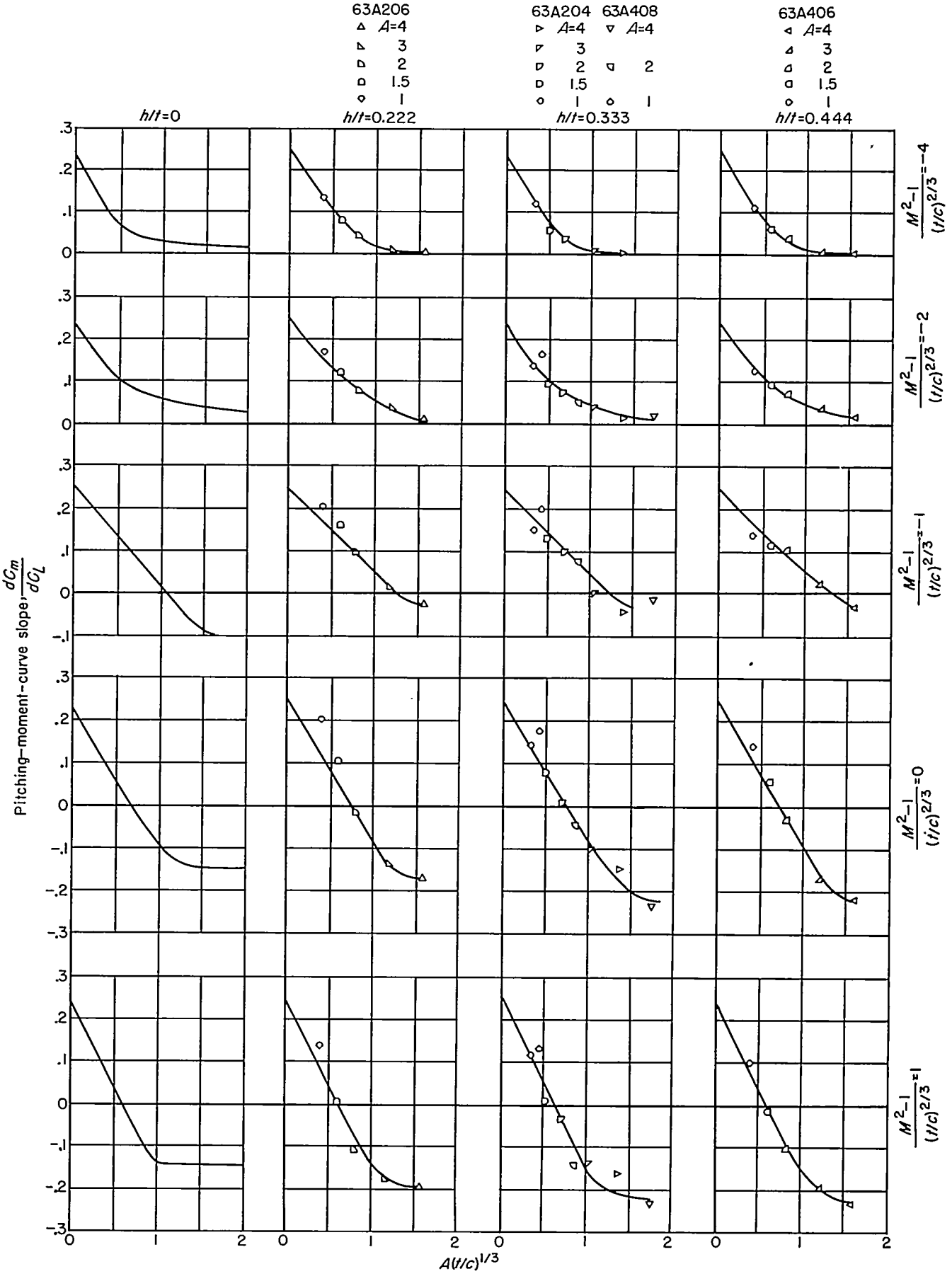

FIGURE 25.—The correlation of pitching-moment-curve slope at $\frac{\alpha}{t/c}=0$ for the cambered wings.

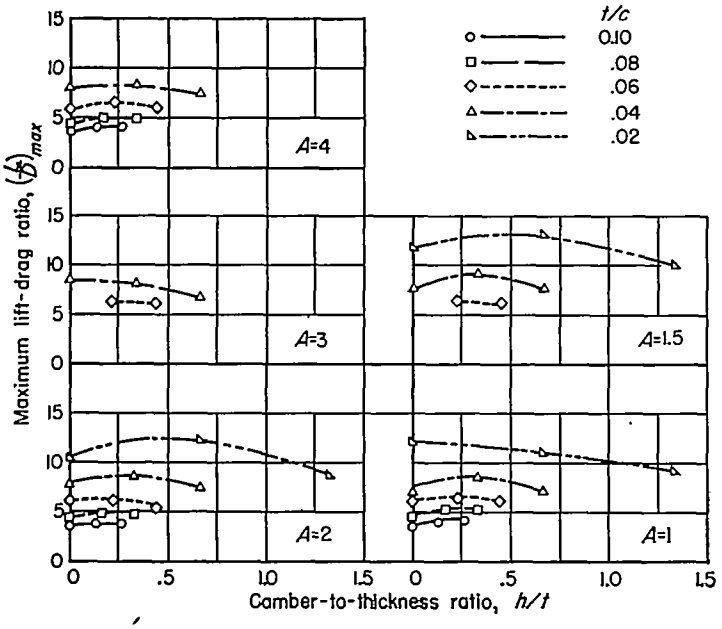

FIGURE 26.—The variation of maximum lift-drag ratio with camber-to-thickness ratio at $M=1$.

coefficients, the data could be presented in a concise manner effectively displaying the wing characteristics for both large and small aspect ratios.

At $M=1$ a linear variation of force and moment coefficients with aspect ratio was found to be a universal property for symmetrical wings having values of $A(t/c)^{1/3}$ less than about 1, while for larger values of $A(t/c)^{1/3}$ an asymptotic approach toward two-dimensional flow independent of aspect ratios was indicated. As a consequence of this result it might be concluded that slender-body concepts apply for rectangular wings at $M=1$, provided the geometric parameter $A(t/c)^{1/3}$ is less than unity. A corresponding evaluation of the limiting value of the speed parameter $\frac{M^2-1}{(t/c)^{2/3}}$ at transonic speeds was not obtained. However, some remarks concerning this parameter for two-dimensional flow expansion is given in the appendix.

AMES AERONAUTICAL LABORATORY
NATIONAL ADVISORY COMMITTEE FOR AERONAUTICS
MOFFETT FIELD, CALIF., *Dec. 17, 1951*

APPENDIX A

ON THE LIMITATIONS OF LINEARIZED THEORY FOR SIMPLE FLOW EXPANSION AT TRANSONIC SPEEDS

The general requirement for linearization of the potential equation of steady flow is that either of the parameters $\frac{\tau}{(M^2-1)^{3/2}}$ or $A\tau^{1/3}$ be much less than 1. In the data correlation of this report it was shown that linearized theory appeared to be valid at $M=1$ (for the wings tested) whenever $A(t/c)^{1/3} \leqq 1$. A corresponding result for the speed parameter $\frac{M^2-1}{(t/c)^{2/3}}$ was not obtained. However, it is interesting to note that a limit for two-dimensional linearized theory can be obtained from a consideration of two-dimensional flow expansion at transonic speeds.

The characteristic solution of equation (2) is the following

$$\left.\begin{aligned} w=\frac{2[(\gamma+1)M^2u+M^2-1]^{3/2}}{3(\gamma+1)M^2}+C \\ u>\frac{1-M^2}{(\gamma+1)M^2} \end{aligned}\right\} \tag{A1}$$

where C is an arbitrary constant and the value

$$u=\frac{1-M^2}{(\gamma+1)M^2} \tag{A2}$$

is an approximation for the critical Mach number.

For supersonic initial Mach numbers the constant C is evaluated by requiring that $w=0$ when $u=0$ to obtain the following transonic approximation for Prandtl-Meyer flow,

$$\left.\begin{aligned} u-u^*=\frac{(3/2)^{2/3}}{[(\gamma+1)M^2]^{1/3}}(w-w^*)^{2/3} \\ \text{where} \\ u^*=-\frac{M^2-1}{(\gamma+1)M^2} \\ w^*=-\frac{2(M^2-1)^{3/2}}{3(\gamma+1)M^2} \\ M\geqq 1 \end{aligned}\right\} \tag{A3}$$

Equation (A3) can be expanded by the binomial theorem to obtain two different series expansions, depending on whether w^2 is greater than or less than w^{*2}. Under the assumption that $C_p=-2u$, the following is obtained

$$\left.\begin{aligned} C_p=-\frac{2w}{\sqrt{M^2-1}}+\frac{(\gamma+1)M^2}{2(M^2-1)^2}w^2-\frac{[(\gamma+1)M^2]^2}{3(M^2-1)^{7/2}}w^3+\cdots \\ w^2<w^{*2} \end{aligned}\right\} \tag{A4}$$

$$\left.\begin{aligned} C_p-\frac{2(M^2-1)}{(\gamma+1)M^2}=\frac{-2(3/2)^{2/3}}{[(\gamma+1)M^2]^{1/3}}w^{2/3}- \\ \frac{2(2/3)^{4/3}(M^2-1)^{3/2}}{[(\gamma+1)M^2]^{4/3}}w^{-1/3}+ \\ \frac{2(2/3)^{4/3}(M^2-1)^3w^{-4/3}}{9[(\gamma+1)M^2]^{7/3}}+\cdots \\ w^2>w^{*2} \end{aligned}\right\} \tag{A5}$$

with the convergence boundary for these series given by

$$C_p=-2(2^{2/3}-1)\frac{M^2-1}{(\gamma+1)M^2} \tag{A6}$$

A series representation for shock compression can be obtained from equation (8). For weak shocks there is obtained, $(C_p=-2\overline{w})$,

$$C_p=\frac{2\overline{w}}{\sqrt{M^2-1}}+\frac{(\gamma+1)M^2}{2(M^2-1)^2}\overline{w}^2+\frac{10[(\gamma+1)M^2]^2}{32(M^2-1)^{7/2}}\overline{w}^3+\ldots \quad (A7)$$

and for strong shocks

$$C_p=\frac{2(M^2-1)}{(\gamma+1)M^2}-\frac{(\gamma+1)M^2}{(M^2-1)^2}\overline{w}^2-\frac{[(\gamma+1)M^2]^3}{2(M^2-1)^5}\overline{w}^4-\ldots \quad (A8)$$

Equations (A4), (A7), and (A8) represent the pressure coefficient by infinite series involving ascending integer powers of the flow deflection with the first terms representing first-order theory. However, equation (A5), which applies if $C_p>-2(2^{2/3}-1)\frac{M^2-1}{(\gamma+1)M^2}$, involves descending fractional powers with the first term varying nonlinearly as the 2/3 power. These results suggest that a limit for linearized two-dimensional-flow theory at slightly supersonic speeds is given by equation (A6). At subsonic speeds linear theory could not be expected to apply above the critical Mach number. These estimated limits for linear theory are shown in figure 27.

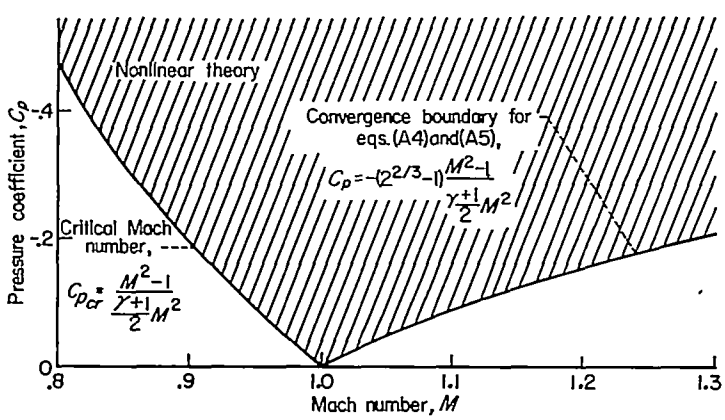

FIGURE 27.—Estimated transonic limits of linearized theory for two-dimensional flow expansion.

The practical limit for linearized theory, of course, depends on one's tolerance for error. It can be shown that this convergence boundary corresponds approximately to a line of constant-percent error for linearized theory. Consider a flow deflection corresponding to the convergence boundary, that is,

$$w=|w^*|=\frac{2}{3}\frac{(M^2-1)^{3/2}}{(\gamma+1)M^2}$$

The corresponding linearized result for the pressure coefficient is

$$C_p=-\frac{4}{3}\left[\frac{M^2-1}{(\gamma+1)M^2}\right] \quad (A9)$$

and the second-order result based on equation (A3) is

$$C_p=-2(2^{2/3}-1)\frac{M^2-1}{(\gamma+1)M^2}-\left[\frac{2}{3}-(2^{2/3}-1)^2\right]\frac{(M^2-1)^3}{[(\gamma+1)M^2]^2} \quad (A10)$$

For Mach numbers near 1 the second term of the above equation is negligible when compared with the first term and equation (A9) is approximately 13 percent greater than equation (A10). Hence, linearized theory is approximately 13 percent in error at the convergence boundary shown in figure 27.

REFERENCES

1. Nelson, Warren H., and McDevitt, John B.: The Transonic Characteristics of 22 Rectangular, Symmetrical Wing Models of Varying Aspects Ratio and Thickness. NACA TN 3501, 1955. (Supersedes NACA RM A51A12)
2. Nelson, Warren H., and Krumm, Walter J.: The Transonic Characteristics of 38 Cambered Rectangular Wings of Varying Aspect Ratio and Thickness as Determined by the Transonic-Bump Technique. NACA TN 3502, 1955. (Formerly NACA RM A52D11)
3. von Kármán, Theodore: The Similarity Law of Transonic Flow. Jour. Math. and Phys., vol. XXVI, no. 3, Oct. 1947, pp. 182–190.
4. Oswatitsch, K.: A New Law of Similarity for Profiles Valid in the Transonic Region. R. A. E. TN 1902 (British), 1947.
5. Kaplan, Carl: On Similarity Rules for Transonic Flows. NACA Rep. 894, 1948. (Formerly NACA TN 1527)
6. Berndt, Sune B.: Similarity Laws for Transonic Flow Around Wings of Finite Aspect Ratio. Kungl. Tekniska Högskolan. Stockholm. Institutionen for Flygteknik. Tech. Note 14, Feb. 20, 1950.
7. Spreiter, John R.: Similarity Laws for Transonic Flow About Wings of Finite Span. NACA TN 2273, 1951.
8. McDevitt, John B.: A Correlation by Means of the Transonic Similarity Rules of the Experimentally Determined Characteristics of 22 Rectangular Wings of Symmetrical Profile. NACA RM A51L17b, 1952.
9. McDevitt, John B.: A Correlation by Means of Transonic Similarity Rules of the Experimentally Determined Characteristics of 18 Cambered Wings of Rectangular Plan Form. NACA RM A53G31, 1953.
10. Busemann, Adolf: Application of Transonic Similarity. NACA TN 2687, 1952.
11. Spreiter, John R.: On the Application of Transonic Similarity Rules to Wings of Finite Span. NACA Rep. 1153, 1953. (Formerly TN 2726)
12. Harder, Keith C.: Transonic Similarity Rules for Lifting Wings. NACA TN 2724, 1952.
13. Liepmann, Hans Wolfgang, and Puckett, Allen E.: Introduction to Aerodynamics of a Compressible Fluid. John Wiley and Sons, Inc., New York, 1947.
14. Loftin, Laurence K., Jr.: Theoretical and Experimental Data for a Number of NACA 6A-Series Airfoil Sections. NACA Rep. 903, 1948.
15. DeYoung, John, and Harper, Charles W.: Theoretical Symmetric Span Loading at Subsonic Speeds for Wings Having Arbitrary Plan Form. NACA Rep. 921, 1948.
16. Jones, Robert T.: Properties of Low-Aspect-Ratio Pointed Wings at Speeds Below and Above the Speed of Sound. NACA Rep. 835, 1946. (Formerly NACA TN 1032)
17. Guderley, Gottfried, and Yoshihara, Hideo: Two-Dimensional Unsymmetric Flow Patterns at Mach Number One. Wright Air Development Center, Tech. Rep. 6683, Jan. 1952.

18. Liepmann, H. W., and Bryson, A. E., Jr.: Transonic Flow Past Wedge Sections. Jour. Aero. Sci., vol. 17, no. 12, Dec. 1950, pp. 745–755.
19. Vincenti, Walter G., and Wagoner, Cleo B.: Transonic Flow Past a Wedge Profile With Detached Bow Wave—General Analytical Method and Final Calculated Results. NACA TN 2339, 1951.
20. Mellenthin, Jack A.: The Flow About a Section of a Finite-Aspect-Ratio NACA 0015 Airfoil on a Transonic Bump. NACA TN 3036, 1953.
21. Abbott, Ira H., von Doenhoff, Albert E., and Stivers, Louis S., Jr.: Summary of Airfoil Data. NACA Rep. 824, 1945.
22. Guderley, G., and Yoshihara, H.: The Flow Over a Wedge Profile at Mach Number 1. Jour. Aero. Sci., vol. 17, no. 11, Nov. 1950, pp. 723–735.

TABLE I.—VALUES OF THE GEOMETRIC PARAMETER $A(t/c)^{1/3}$ FOR THE WING MODELS TESTED

A	t/c	$A(t/c)^{1/3}$
6	0.10	2.784
6	.08	2.536
6	.06	2.352
4	.10	1.856
4	.08	1.724
4	.06	1.568
4	.04	1.368
3	.04	1.026
2	.10	.928
2	.08	.862
2	.06	.784

A	t/c	$A(t/c)^{1/3}$
2	0.04	0.684
2	.02	.542
1.5	.04	.513
1.5	.02	.407
1	.10	.464
1	.08	.431
1	.06	.392
1	.04	.342
1	.02	.271
.5	.04	.171
.5	.02	.136

TABLE II.—NUMERICAL VALUES OF $(t/c)^{1/3}$, $(t/c)^{2/3}$, AND $(t/c)^{5/3}$

t/c	$(t/c)^{1/3}$	$(t/c)^{2/3}$	$(t/c)^{5/3}$
0.12	0.493	0.243	0.0293
.11	.479	.230	.0254
.10	.464	.216	.0217
.09	.448	.201	.0181
.08	.431	.186	.0148
.07	.412	.170	.0118
.06	.392	.154	.0092
.05	.368	.136	.0068
.04	.342	.117	.00468
.03	.311	.097	.00292
.02	.271	.073	.00147

TABLE III.—VALUES OF THE ANGLE OF ATTACK (IN DEGREES) FOR VARIOUS VALUES OF THE RATIO $\frac{\alpha}{t/c}$ (IN RADIANS)

t/c	Angle of attack α, degrees			
	$\frac{\alpha}{t/c}$, 0.5 radian	1.0 radian	1.5 radians	2.0 radians
0.10	2.87	5.73	8.60	--------
.08	2.29	4.58	6.87	--------
.06	1.72	3.44	5.16	6.87
.04	----------	2.29	3.44	4.58
.02	----------	--------	1.72	2.29

U. S. GOVERNMENT PRINTING OFFICE: 1957